INFRARED MULTIPHOTON DISSOCIATION OF GASEOUS IONS STUDIED BY FOURIER TRANSFORM ION CYCLOTRON RESONANCE MASS SPECTROMETRY

BY

CLIFFORD HUNTER WATSON

A DISSERTATION PRESENTED TO THE GRADUATE SCHOOL
OF THE UNIVERSITY OF FLORIDA IN
PARTIAL FULFILLMENT OF THE REQUIREMENTS
FOR THE DEGREE OF DOCTOR OF PHILOSOPHY

UNIVERSITY OF FLORIDA

1986

ACKNOWLEDGEMENTS

Scientific research is rarely conducted by isolated individuals, and this dissertation is no exception. First, I would like to acknowlege Dr. Robert Hanrahan for the use of his Gear integrator program which was the basis of the kinetic modeling described in Chapter 6. The excellent technical facilities of the machine shop, electronic shop, and glass blowing shop and the help of their skillful personnel have greatly facilitated this work. I am particularly thankful to Mr. J.D. McMillan in the machine shop who was never too busy to discuss the design of new experimental hardware or to transform that design to a working product.

Next, I would also like to acknowledge Dr. Samuel Colgate who was instrumental in my decision to enter the area of physical chemistry. The knowledge and exuberance he exhibited in a course in thermodynamics early in my career at the University of Florida filled me with a burning desire to study physical chemistry.

I am grateful to my colleagues in the Eyler group for their help and suggestions. In particular, Dr. Gokhan Baykut deserves particular thanks. His scholarly approach to scientific problems and his dedication to his work have been an example to me during these past two years. I have greatly benefitted from the many discussions with him about our

work. In addition, his technical and artistic talents in the preparation of the figures in this dissertation warrant special recognition. And most of all, I have appreciated his friendship over these last years.

Next, I wish to acknowledge my research advisor, Dr. John Eyler, without whom this work would not have been possible. His research funds have enabled me to devote the last two years exclusively to laboratory research and have made it possible for me to work with state-of-the-art equipment. This funding has also supported my attendance at the annual meetings of the American Society of Mass Spectrometry, which have been a major influence in my development in this area. His editing skills have been of monumental assistance in the transformation of my rough drafts to final written form. I am extremely grateful to him for his help and guidance over the last three years. Last but not least, I have greatly appreciated his encouragement of my goals and confidence in my abilities.

The person to whom I am most grateful is my wife, Sonja Rasmussen. She has always been there, whether I needed motivation to keep working or encouragement to take a break. She is my best friend and the love of my life.

TABLE OF CONTENTS

Abstract of Dissertation Presented to the Graduate School of the University of Florida in Partial Fulfillment of the Requirements for the Degree of Doctor of Philosophy

INFRARED MULTIPHOTON DISSOCIATION OF GASEOUS IONS STUDIED BY FOURIER TRANSFORM ION CYCLOTRON RESONANCE MASS SPECTROMETRY

By

Clifford Hunter Watson

December 1986

Chairman: Dr. John Eyler
Major Department: Chemistry

Infrared multiphoton dissociation (IRMPD) provides a versatile method of obtaining energetics and structural information about gaseous ions. This method is facilitated by the use of Fourier transform ion cyclotron resonance mass spectrometry, because the length of time which ions can be trapped allows the sequential absorption of many infrared photons. The ions were irradiated by a grating-tuned continuous wave CO_2 laser. The relative photodissociation cross section was observed to vary as a function of laser wavelength for a series of propane- and butanediols. The use of the phenomenon of wavelength-dependence as a possible method of isomeric differentiation was explored.

Another approach to isomeric differentiation involved the production of different photoproducts. This method was used to investigate a series of ions having the same

empirical formula arising from different ether and ester precursors.

Infrared multiphoton dissociation and collision induced- dissociation (CID) were compared for molecular ions and protonated molecules of substituted ethyl- and propyl-amines. While the sole fragment ion produced by IRMPD was always observed in the CID daughter spectrum, this ion was not always the most abundant.

The collisional quenching of vibrationally excited ions by various buffer gases was investigated. The corresponding neutral parent molecule was observed to have a very high quenching efficiency. A kinetics model was presented to explain collisional deactivation.

Moderate mass ions (m/z 300-600) formed by laser desorption (LD) were observed to photodissociate. The combination of IRMPD and LD provides information about both molecular weight and structure of compounds that are difficult to analyze with traditional methods.

CHAPTER 1
INTRODUCTION

Mass spectrometric methods (Watson, J.T., 1985) provide a wide range of information about chemical compounds and have been applied in an increasing number of chemical subdisciplines in recent years. All branches of chemistry, analytical (Burlingame et al., 1986), inorganic (Eyler and Richardson, 1985), organic (Chapman, 1985), and physical (Lindholm and Asbrink, 1985) benefit by this microanalysis technique. Mass spectrometry, however, is by no means used solely by the chemist. Other areas, such as biomedical science (Gaskell, 1986), environmental science (Karasek, 1985), and the health and life sciences (Kambara, 1985), just to name a few, also utilize this technique for both quantitative and qualitative analysis. From its humble beginning as a single stage mass analyzer $(MS)^1$ through the development of various modern tandem $(MS)^2$ and hybrid mass spectrometers $(MS)^n$, where n is the number of stages or mass spectrometers bolted together, mass spectrometry has yielded a wealth of chemical information.

The types of information that are readily available to the mass spectroscopist include energetic, reaction rate and mechanistic, and various spectroscopic data. Typical energetic data include determination of ionization potentials (Mark, 1984), heats of formation (Lossing and

Holmes, 1984), and electron affinities (Grimsrud et al., 1985). The measurement of reaction rates and mechanistic studies are interesting in and of themselves (Prisant et al., 1984) and in unfavorable cases can lead to difficulties in spectral interpretation (McLafferty, 1980) unless adequately considered. Spectroscopic information from multiphoton ionization (Pandolfi et al., 1983), two-laser techniques (Kuehlewind et al., 1984), and photodissociation (Thorne, 1983) can yield valuable information about ion fragmentation pathways, internal energy distributions, and structures.

The main burden of mass spectrometry, however, has been the identification and quantification of unknown samples. The accurate mass measurements now routinely available on many high resolution instruments can determine easily the molecular composition from the ion's mass-to-charge ratio (m/z). However, the often important problem of determining, or at least differentiating between, the structures of several isomeric forms of an ion with a given mass-to-charge ratio has not yet been solved completely. Several approaches to the problem which are successful with certain classes of ions have been developed. Many of these techniques relied on the development of multistage mass spectrometers $(MS)^{n>1}$, where an ion of a particular m/z ratio can be isolated and studied. The most widespread of these is the technique of collision-induced dissociation (CID), one of the processes occurring in collisional activation (CA) spectroscopy (Cooks, 1978; Levsen and

Schwatrz, 1983), which has been applied not only in various magnetic sector instruments (Cooks, 1978; Levsen and Schwartz, 1983) but also in the triple quadrupole mass spectrometer (Yost and Enke, 1979) and in Fourier transform mass spectrometers (Cody and Freiser, 1982; Cody et al. 1982a,b).

An alternate approach to isomeric differentiation involves the use of bimolecular ion/molecule reactions to distinguish between various ionic structural isomers based on their differing reactivity. This approach has most often employed an ion cyclotron resonance (ICR) mass spectrometer (Baldeschwieler, 1968; Lehman and Bursey, 1976). Many of the species investigated have been small hydrocarbon ions (Gross et al., 1977; Jackson et al., 1977; Ausloos, 1981; Eyler and Campana, 1983/1984). A similar technique involving the use of low-energy reactive collisions has also recently been reported (Fetterolf et al., 1984) for isomeric differentiation of $C_3H_3^+$ isomers in a triple quadrupole mass spectrometer.

The use of conventional light sources or uv/visible lasers to photodissociate gaseous ions of interest is another quite promising approach to isomeric differentiation (Dunbar, 1979). For favorable cases, the photodissociation spectrum of various structural isomers can be obtained (Dunbar, 1984; Mukhtar et al., 1982; Mukhtar et al., 1981) and used, for example, to probe the structure of ion/molecule reaction products (Orth and Dunbar, 1982). In order to observe photodissociation, the ions of interest

must possess an allowed transition in the range of output wavelengths available from the light source and must also have available energetically allowed dissociation pathways from the excited states which are reached upon photon absorption. While these conditions are met for a wide range of ions, there are other classes for which they do not hold and, hence, for which this approach to isomeric differentiation is not possible.

Several groups have reported work involving photodissociation of gaseous ions with relatively low-powered infrared (CO_2) lasers (continuous wave (CW) and pulsed) (Bomse et al., 1978; Rosenfeld et al., 1983; Lev and Dunbar, 1983; Hughes and March, 1982). Again, most of these studies have been carried out in ICR mass spectrometers, where ions can be trapped for long periods of time during which they may sequentially absorb many infrared (IR) photons. Often 5-20 infrared photons must be absorbed before the ion dissociates (Thorne and Beauchamp, 1984). Since ion photodissociation can be followed as a function of the relatively limited range of CO_2 laser wavelength, this type of experiment raises the possibility of isomeric differentiation based on the observed infrared photodissociation spectrum. Indeed, at least two reports have been published on the subject, one dealing with $C_3F_6^+$ photodissociation (Bomse and Beauchamp, 1981), and one with $C_7H_7^-$ photodetachment (Wight and Beauchamp, 1979) which also can be induced by infrared radiation. Is should be noted, however, that the former work did not actually distinguish between $C_3F_6^+$ isomers, but

rather found that isomeric ions of this empirical formula produced from several sources showed the same infrared multiphoton dissociation spectra, apparently because the ions rearranged to a common structure on a time scale shorter than that of the sequential infrared photon absorption which led to dissociation.

This exciting approach for differentiating structural isomers of gaseous ions by measuring the amount of photodissociation as a function of laser wavelength and constructing a photodissociation spectrum was particularly attractive as the work described in this dissertation began. Various aspects and outgrowths of this work are addressed in the following chapters which demonstrate the usefulness of infrared multiphoton dissociation to obtain both structral and energetic information on selected gaseous ions.

The infrared multiphoton dissociation spectra for isomeric ions of protonated propane and butane diols are presented in Chapter 3. These diols were observed to photodissociate with loss of a water molecule, and while no drastic differences in spectral fine structure were observed for these protonated diols, the observed photodissociation cross section varied widely, reflecting the different isomeric structures.

Infrared multiphoton dissociation of neutral molecules has been well studied (Black et al., 1977, 1979); however, there are a number of significant differences between dissociation of neutrals (or ions) brought about by high-

power, pulsed CO_2 lasers and the dissociation of ions trapped in an ICR mass spectrometer subjected to irradiation from a chopped or gated CW CO_2 laser of relatively low power. In the latter process, if the rate of absorption of photons by the trapped ions exceeds the rates of radiative and collisional relaxation, increasing amounts of vibrational energy are accumulated in the ion, eventually resulting in its dissociation. The best discussion of the many aspects of this type of experiment has been given by Thorne and Beauchamp, 1984, who note two general cases involving small and large ions. For small ions, resonant absorption of one or more infrared photons could be expected (and was suggested experimentally) before eventual absorption of numerous photons into the quasicontinuum complete the energy input necessary to produce dissociation. Large ions already possess a density of states sufficiently high that even absorption of the first infrared photon was expected to be into the quasicontinuum.

For almost all ions studied, both here and elsewhere (Thorne and Beauchamp, 1984), the slow sequential absorption of infrared photons by the trapped ions occurred in a time period of many milliseconds. During this relatively long irradiation period, complete randomization of energy throughout all of the normal modes of the ion was postulated, resulting in dissociation via the lowest activation energy pathway, as soon as sufficient energy had been accumulated in the ion. This point has also been discussed for photodissociation of neutrals (Lee and Shen,

1976). Such dissociation via the channel of lowest activation energy leads to the possibility of a second means of isomeric differentiation with IR multiphoton photodissociation (IRMPD). Instead of noting the wavelength dependence of ionic dissociation for different isomers, which may not be significant as the ions approach the large molecule limit, one might observe differences in the dissociation products of different isomers, since different structures might be expected to possess different lowest energy dissociation pathways. One example of this approach, where different dissociation products were observed for isomeric proton-bound alcohol dimers, has been reported (Bomse and Beauchamp, 1981).

This method of isomeric differentiation is reported in Chapter 4 for a series of oxygen-containing ions obtained from different precursors. The appearance of different photofragments is used to distinguish structural isomers of gaseous ions. The different photofragments reflect the difference in the height of the lowest energy of activation barrier leading to dissociation for ions of different structures. For a variety of ions the appearance of different photofragments can be used to establish the presence of different structures. Based on the structure of the precursor and observed fragmentation pattern, the identities of the various structures are postulated.

For the types of ions studied here, one photodissociation pathway was observed which corresponded to the dissociation pathway of lowest activation energy. The

photodissociation process may be thought of as analogous to the low-energy collision-induced dissociation. In both dissociation techniques the ions become energetically activated, and if the activated ion has sufficient energy dissociation occurs. Presented in Chapter 5 is a comparison of infrared multiphoton dissociation and collision-induced dissociation for selected ethyl and propyl substituted amines. For each ion studied, the fragment ion produced by infrared multiphoton dissociation was also observed as a fragment ion in the collision-induced dissociation mass spectrum. For several interesting cases the sole fragment ion resulting from infrared multiphoton dissociation was not the most abundant fragment ion produced by collision induced dissociation. These differences are explained in terms of a loose versus a tight transition state of the dissociating ion, where not only energetic barriers but also entropic barriers must be overcome.

Many theories have been advanced to explain the multiphoton dissociation of neutral molecules, most often produced by irradiation with high-power, pulsed CO_2 lasers (Ambartzumian and Letkhov, 1977; Bagratashvili et al., 1983). Due to the anharmonicity of normal mode vibrations, the distance between discrete energy levels decreases with increasing energy, and thus it is difficult to explain multiple photon absorption phenomena in a monochromatic laser field simply by assuming a step-by-step progression up the vibrational energy ladder. Recent theories agree that in small molecules, a multiple photon absorption process

starts with the resonant absorption of one photon, which is sometimes followed by two or three more "near-resonance" absorptions. Tamir and Levine, 1977, suggest that two anharmonic-coupled vibrational energy ladders are involved in multiple photon dissociation processes. The first mode absorbs a photon form the laser field and transfers a certain amount of energy to a second accepting energy ladder intramolecularly. This transfer clears the first mode for the next resonant absorption, after which a part of the energy is again transferred to the second ladder. Thus the degree of excitation increases in the second mode, resulting eventually in sufficient excitation to cause photodissociation. Freidman, 1979, assumes a near-resonant absorption of the first photon by a pumped mode and an intramolecular transfer of this energy to a low-lying quasicontinuum, which clears the first mode for another absorption process. Aother theory (Grant et al., 1978) assumes that that the first photon is resonantly absorbed, and rotational compensation allows absorption of additional photons until the quasicontinuum is reached.

Unlike dissociation of ions by light from high-power, pulsed infrared lasers where the pulse width is only a few microseconds, the slow sequential absorption of many infrared photons by low-power infrared lasers results in dissociation only if the rate of photon capture exceeds the rate of photon loss. The irradiated ion may relax by spontaneous emission of a photon or by collisional deactivation. Rates of infrared emission have been estimated

(Dunbar, 1975) to be approximately 1 to 100 s^{-1}. At low pressures ($<10^{-8}$ torr) the radiative deactivation process, in the absence of collisions on the time scale of the experiment, is responsible for the relaxation of vibrationally excited ions. At higher pressures (10^{-7} to 10^{-5} torr) collisional deactivation of highly vibrationally excited ions by the neutral buffer gas becomes more important. The role of collisional quenching is explored in Chapter 6 and a kinetics model is presented which adequately describes this process.

While most of the infrared multiphoton dissociation work to date has concentrated on relatively low molecular weight ions, extensions of this technique to higher molecular weight or nonvolatile compounds have also proven to be very informative as shown in Chapter 7. High molecular weight compounds can often be ionized by the laser desorption technique. Laser desorption is characterized as a soft ionization process (Van Breman et al. 1983) that produces high abundances of molecular or pseudo-molecular ions, with few fragment ions, yielding excellent molecular weight information.

Fragmentation is often desirable in mass spectrometry, however, to provide structural information. Both structural and energetics information can be obtained by irradiating these molecular ions with infrared light and observing the photodissociation pathways. The material presented in Chapter 7 relates the successful combination of laser

desorption and infrared multiphoton dissociation to both ionize and fragment large molecular weight compounds.

The development of Fourier transform ion cyclotron resonance mass spectrometry has greatly facilitated the study of infrared multiphoton dissociation of gaseous ions. Foremost among its abilities are that ions can be trapped for long periods of time and that it is possible to detect an entire mass spectrum in a very short time period. Ions of a particular m/z can be selected by applying various ion ejection pulses to the analyzer cell (discussed further in Chapter 2). Thus multiple mass spectrometric experiments $(MS)_n$ are possible by application of appropriate ejection pulses. Unlike the $(MS)_n$ experiments mentioned above, this is accomplished by manipulating the ions in time rather than through space. Also, the ability to eject ions both before and during laser irradiation allows photodissociation pathways to be determined unequivocally. In the following chapter the essential operating principles of Fourier transform ion cyclotron resonance mass spectrometry will be discussed along with the modifications and laser systems necessary for the study of infrared multiphoton dissociation of gaseous ions.

CHAPTER 2
INSTRUMENTATION

Since development of the Fourier transform ion cyclotron resonance mass spectrometer (Comisarow and Marshal, 1974), many applications which exploit the strengths of this technique have been reported. A recent review article (Laude et al., 1986) summarizes the diversified applications of this relatively new type of mass spectrometry. The advantages of using Fourier transform ion cyclotron mass spectrometry include high resolution mass analysis (Allemann et al., 1983), high molecular weight analysis (Amster et al., 1986), long trapping times (Allemann et al., 1980), and the ability to manipulate the ion population by various ejection techniques (Baykut and Eyler, 1986).

Operation of the commercial Nicolet FT/MS-1000 mass spectrometer, with the exception of sample introduction and ionizing emission current, is entirely under computer control. All data acquisition and processing and the selection of various user-definable experimental sequences are achieved by typing simple commands on the computer's keyboard. The vacuum system and analyzer cell (discussed below) are easily adapted for the study of infrared multiphoton dissociation.

The analyzer cell is of cubic or rectangular geometry, consisting of six electrically isolated stainless steel plates (see Figure 2.1). The three sets of opposite plates serve as trapping, excitation, and detection plates. Only the choice of trapping plates is critical since these must be perpendicular to the magnetic field lines to trap the ions. Once the ions are formed, they are subject to the forces produced by crossed electric and magnetic fields. As a result of the Lorentz force, the ions begin to move in cyclotron motions. The force on an ion of mass m, charge q, and initial velocity v produces an acceleration a, given by Newton's second law and the Lorentz equation,

$$F = ma = q(vxB) \qquad 2.1$$

Substitution of the centripetal acceleration,

$$a = v^2/r = rw^2 \qquad 2.2$$

where r is the cyclotron radius and w is the angular frequency, into equation 2.1 and noting that v = rw results in the cyclotron equation that relates the cyclotron frequency to an ion's m/z (equation 2.3).

$$w = qB/m \qquad 2.3$$

Morgenthaler, 1979, describes the derivation and extensions of these equations in much greater detail. The all cases considered here the charge of an ion, z, will have a value of one.

After formation the ions have random phase and undergo cyclotron motion with the characteristic frequency w, as given by equation 2.3. For this work the magnetic field was produced by a superconducting solenoid magnet with a

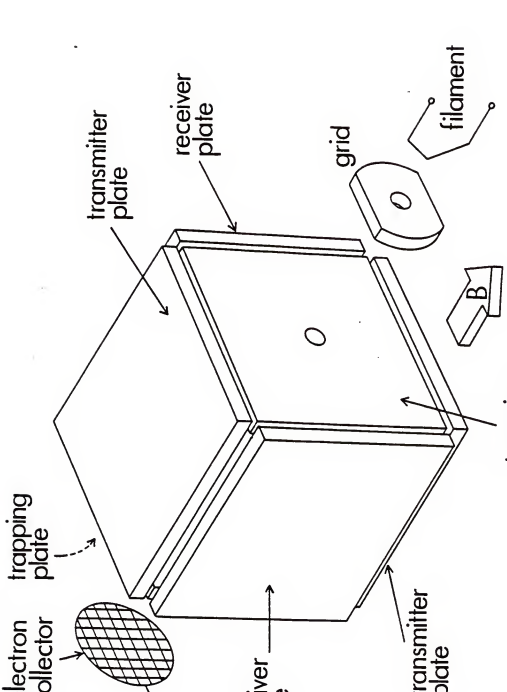

Figure 2.1. Standard cubic analyzer used in Fourier transform ion cyclotron resonance.

constant magnetic field strength of 3 tesla. Given that the charge of an electron, q, is constant, the cyclotron frequency w, is inversely proportional to and determined uniquely by the ion's mass. Detection of the ions is accomplished by application of a swept oscillating voltage in the radio frequency range to the excitation plates, which drives the ions into coherent motion. This coherent motion of ions induces an alternating image current on the cell plates resulting from the cyclotron motion of ions. The image current contains all the frequency information resulting from cyclotron motion when ions with different m/z ratios are present. This behavior has been explained theoretically in terms of a rotating monopole (Comisarow, 1977). The image current is detected on the receiver plates and it is amplified, digitized and stored in the computer's memory where a Fast Fourier Transform (Cooley and Tukey, 1965) converts the time domain data into a frequency spectrum and hence a mass spectrum. Shown in Figure 2.2 is a computer generated time domain spectrum consisting of the sum of two sine waves of frequencies w_1 and w_2 with an exponential damping to represent collisional dephasing of the coherent ion motion resulting from collisions between the ions and neutral background molecules present in the vacuum chamber. By performing a Fourier transform on this time domain data one extracts the frequency information and constructs a frequency domain spectrum such as the one shown in Figure 2.3. The two peaks correspond to the signals having frequencies w_1 and w_2 used to construct the time

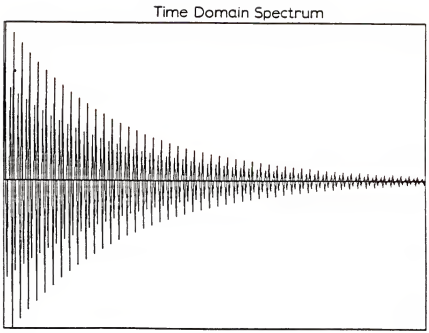

Figure 2.2. Computer-simulated time domain spectrum with exponential decay (abscissa is time; ordinate is ion signal).

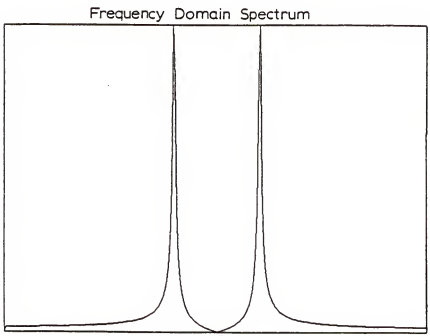

Figure 2.3. Computer-simulated frequency domain spectrum obtained by fast Fourier transform of the data shown in Figure 2.2 (abscissa is frequency; ordinate is ion signal).

domain spectrum. From the frequency spectrum produced by ions in the Fourier transform ion cyclotron resonance mass spectrometer, one also has the mass spectrum since frequency and mass are inversely proportional (see equation 2.3).

A typical pulse sequence that controls the ion formation, ion manipulation, and ion detection is shown in Figure 2.4. A quench pulse clears the cell of ions to begin a new experiment. This is accomplished by applying a +15 volt potential to one trap plate and a -15 volt potential to the opposite trap plate. Positive ions are accelerated to the negative plate and negative ions are accelerated to the positive plate, where both are neutralized upon collision with the respective plate. Electrons accelerated to typically 50 eV ionize the sample for typically 5 milliseconds during the electron beam pulse. The distribution of ions with various masses can be manipulated by up to 6 ejection pulses. An ion of known m/z can be ejected from the cell by application of a single frequency that corresponds to the cyclotron frequency. The ion absorbs energy from the resonant field and moves to a larger and larger cyclotron radius until it strikes a cell plate and is neutralized. Sweeping over a given frequency range during an ejection pulse can remove a range of ions whose mass-to-charge ratios correspond to those frequencies. For instance, an ion of a particular m/z can be selected for study by application of the appropriate ejection pulses to sweep out all other masses less than or greater than the one of interest. To detect the ions, an attenuated fast

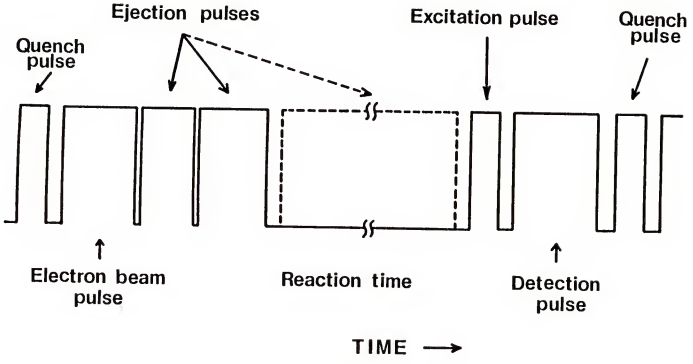

Figure 2.4. Generalized pulse sequence employed in Fourier transform ion cyclotron resonance mass spectrometry (ordinate is voltage).

frequency sweep of sufficient amplitude to drive the ions into coherent motion without ejecting them from the cell is applied to the excitation plates. The resulting image current of the coherent ion motion appearing on the detection plates is amplified and digitized. The entire sequence can be performed repeatedly to acquire a signal-averaged mass spectrum.

Shown in Figure 2.5 is a schematic representation of the Fourier transform ion cyclotron resonance mass spectrometer. The vacuum chamber housing the analyzer cell passes through the bore of a 3 tesla superconducting solenoid magnet. The analyzer cell is located in the center of the magnet where the magnetic field has the highest homogeneity. A background pressure of less than 10^{-8} torr is maintained by a six-inch diameter oil diffusion pump and the vacuum system is also baked-out overnight at 250 ^{o}C.

Liquid and gaseous samples are introduced into the high vacuum by mean of precision leak valves. Liquid samples are frozen to liquid nitrogen temperatures and the air above the liquid is evacuated through the inlet system with a four-inch diameter oil diffusion pump. The samples are allowed to thaw. Several of these freeze-pump-thaw cycles remove any residual air trapped inside the liquid before mass analysis.

Solid samples can be analyzed by two methods. The sample can be placed on a solids insertion probe, inserted into the vacuum chamber, and heated to as high as 250 ^{o}C to drive vapors from the solid. These vapors, once produced,

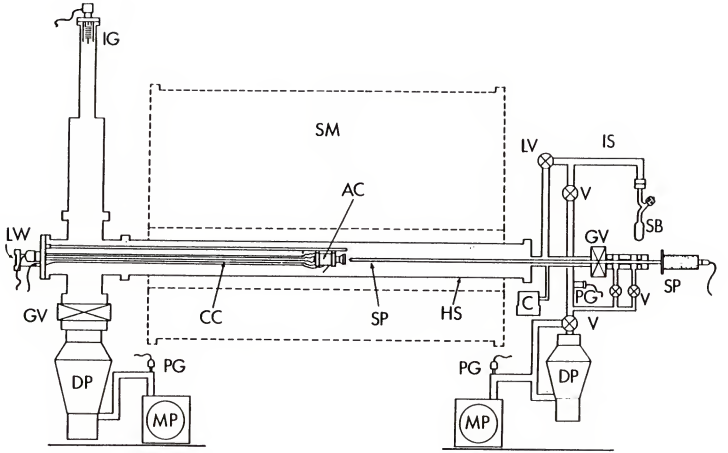

Figure 2.5. Schematic representation of the FTICR. AC = analyzer cell; CC = cell cables; DP = diffusion pump; GV = gate valve; HS = vacuum housing; IG = ionization gauge; IS = inlet system; LV = leak valve; LW = ZnSe window; MP = mechanical pump; PG = pressure gauge; SB = sample bulb; SM = solenoid magnet; SP = solids probe; V = valve.

are ionized by electron impact and mass analyzed. Alternatively the sample can be vaporized and ionized by the laser desorption technique. This method is discussed later in Chapter 7.

The standard analyzer cell supplied with the commercial Nicolet instrument has been modified to allow laser irradiation of the ions. Initially, the rear trapping plate was replaced by one having a 1.5 cm diameter hole that was covered by a fine copper mesh of 90% transparency (see Figure 2.6). From the principles of electrostatics, ions a distance greater than the spacings of the mesh effectively "see" a solid surface. The use of this trapping plate did not significantly degrade the trapping ability. To irradiate the ions a sodium chloride window supported on O-ring seals fastened upon a hollow tube was inserted through the solids probe vacuum insertion lock. Light from an Apollo 570 grating-tuned, continuous wave (CW) carbon dioxide laser entered the vacuum chamber through the window and traversed the tube to reach the cell (see Figure 2.7). Two NaCl windows were used as beam splitters and two fractions of the beam could be extracted for wavelength and power monitoring. A helium-neon laser could be aligned colinearly with the "invisible" infrared beam to facilitate alignment of the laser optics. The Apollo CW CO_2 laser has a maximum power output of 50 watts at a wavelength of 10.61 microns. After loss from various optics the amount of light reaching the ions is attenuated by a factor of 10.

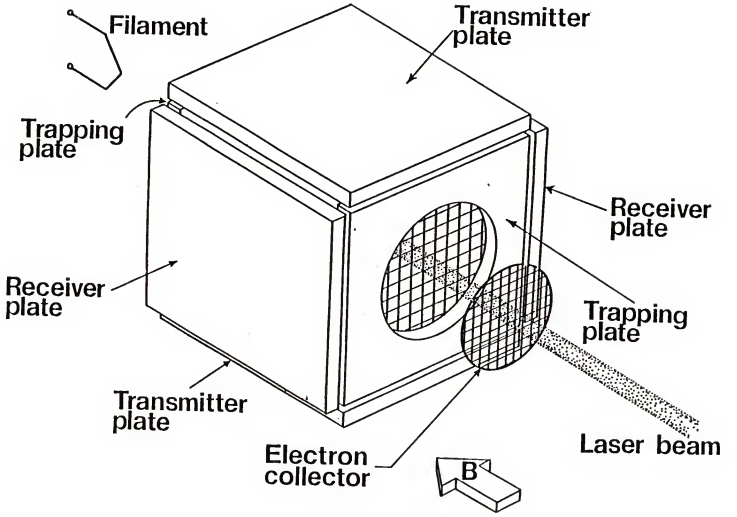

Figure 2.6. Cubic FTICR cell with modified trapping plate to allow irradiation of trapped ions.

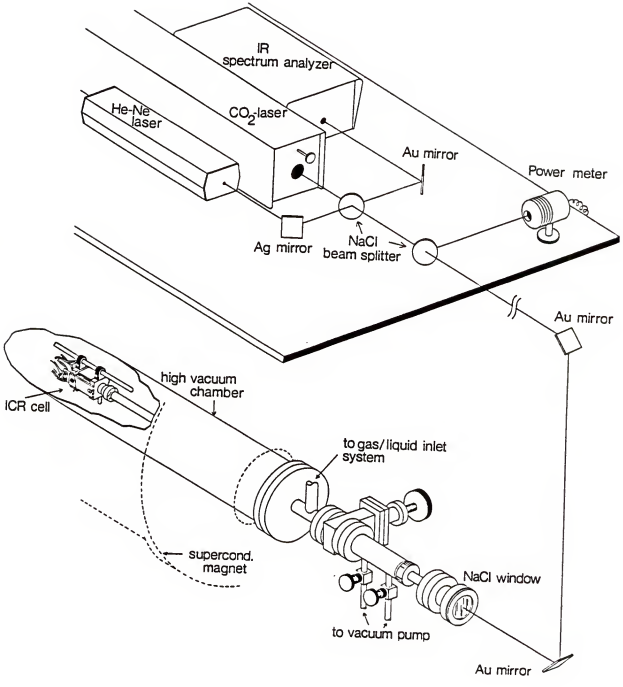

Figure 2.7. Laser table and cut-away view of the relevant portions of the FTICR instrumentation. The He-Ne laser was used only for alignment of the CO_2 laser.

Later modifications of the analyzer cell consisted of removing one of the excitation plates and replacing it with one that also had a 1.5 cm diameter hole. A stainless steel reflector was spot welded to this plate to reflect the laser beam into the cell (see Figure 2.8). A zinc selenide window mounted on the cell support flange allowed light to enter the vacuum chamber where it impinged on the reflector and was reflected into the cell (see Figure 2.9). This arrangement allowed the study of ions formed not only from gases and liquids, but also from solid samples introduced on the solids insertion probe.

For the work presented in Chapters 3-6, the Apollo CO_2 laser was used exclusively. In the studies described in Chapter 7, a Lumonics TE 860 pulsed CO_2 grating-tuned laser was used to perform sample ionization by laser desorption. This laser was also used for limited photodissociation studies involving laser-desorbed ions. The Lumonics laser had a maximum output power of 2.6 Joules produced in a one-microsecond pulse. The beam profile consisted of a 2 X 3 cm. rectangular shape; the laser intensity was observed to be uniformly distributed as indicated by burn patterns on thermal paper. The beam was focused by a ZnSe lens for the laser desorption studies. The power density impinging on the sample was estimated to be greater than 10^8 watts/cm^2.

The purpose of this chapter was to give the reader a brief overview of FTICR and a feeling for the types of experiments and experimental methods discussed in the

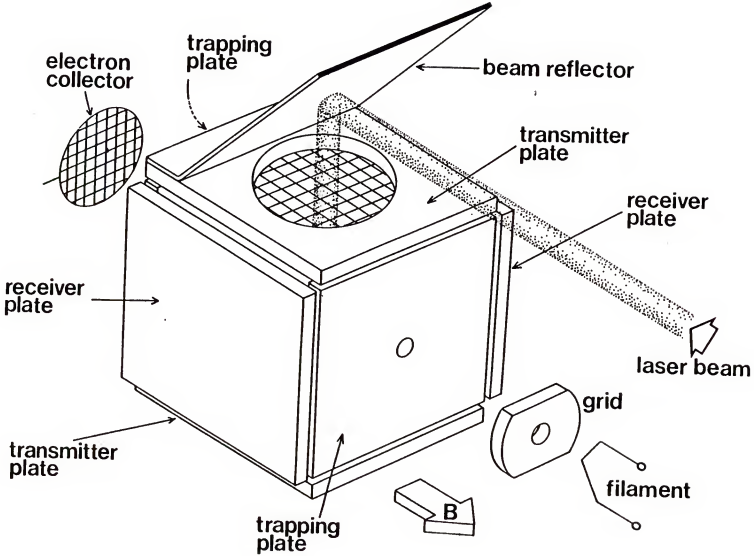

Figure 2.8. Cubic FTICR cell with modified transmitter plate for irradiation of trapped ions.

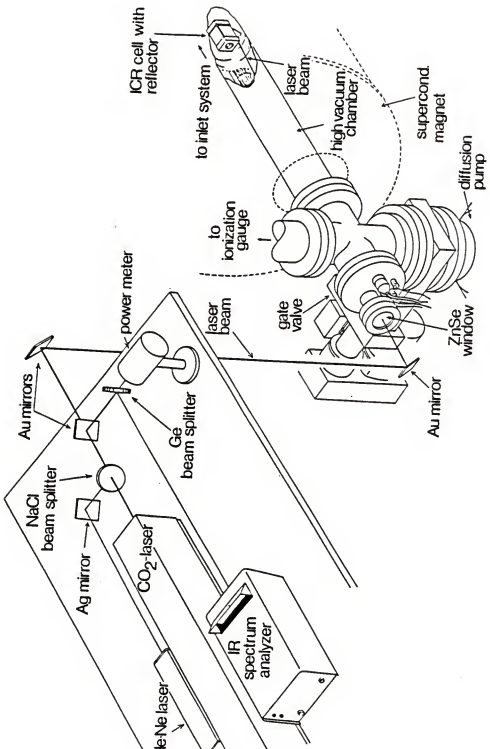

Figure 2.9. Laser table and cut-away view of relevant portions of the FTICR instrumentation.

following chapters. Included in each of the following chapters are experimental sections that describe in much greater detail the pertinent experimental set-ups and procedures.

CHAPTER 3
ISOMERIC DIFFERENTIATION OF PROTONATED PROPANE AND BUTANE DIALCOHOLS BY INFRARED MULTIPHOTON DISSOCIATION WAVELENGTH DEPENDENCE

Two photochemical methods of isomeric differentiation are discussed in this and the following chapter. Both involve irradiating ions trapped within the ICR cell with infrared light from a continuous wave CO_2 laser. Upon irradiation the ions sequentially absorb infrared photons until sufficient energy is accumulated for dissociation to occur. The energy randomizes among all normal modes of the molecule, and there is a certain statistical probability that all quanta will converge upon one normal mode. As the energy "samples" each normal mode, the lowest activation energy barrier leading to dissociation will eventually be exceeded and the ion will dissociate along this lowest activation energy pathway. One might expect that isomeric ions would have different lowest energy dissociation pathways and that the appearance of different photofragments would reflect different ion structures. For certain classes of compounds this is indeed the case; this method of isomeric differentiation is presented in the following chapter. However, another method of isomeric differentiation is needed for isomeric ions which produce similar photofragments. One alternative approach discussed below is to measure the amount of photodissociation as a

function of wavelength and to construct a "photodissociation spectrum". Differences in the infrared absorption cross section reveal a unique photodissociation spectrum for each isomeric ion. Thus, isomeric differentiation is achieved by comparison of these different spectra.

The fraction of ions which photodissociate is given by

$$I/I_o = \exp(-kt) \qquad 3.1$$

where I is the ion signal after irradiation for a period of time, t, I_o is the corresponding signal without irradiation and k is the rate constant for photodissociation. For many classes of ions the photodissociation rate constant, k, has a linear dependence on laser irradiance and can be expressed in terms of a phenomenological photodissociation cross section, σ (Thorne and Beauchamp, 1984)

$$k = \sigma\bar{\Phi} \qquad 3.2$$

where $\bar{\Phi}$ is the photon flux. The photodissociation cross section is a function of wavelength and can be expressed as (Morgenthaler, 1979)

$$\sigma(\lambda) = \frac{c \ln(I_o/I)}{\lambda E(\lambda)} \qquad 3.3$$

where λ is the wavelength, $E(\lambda)$ is the irradiation energy and c is the overlap factor. One can calculate the photodissociation cross section for particular laser wavelengths by measuring the ion signal with (I) and without (I_o) laser irradiation at a given wavelength and laser power.

For high-power megawatt pulsed lasers the relationship between the gas-phase optical absorption of the neutral's

spectrum and the photodissociation spectrum of the corresponding ion have been established (Ambartzumian and Letokhov, 1977; Hartford, 1978). Several photodissociation spectra have been reported using low-power continuous wave CO_2 lasers. The photodissociation spectrum of the perfluoropropylene ion using low-power CO_2 lasers has been shown to correlate with the infrared spectrum of neutral perfluoropropylene (Woodin et al., 1979). A similar correlation was also observed for the diethylether ion and neutral (Bomse et al., 1979). The diethylether photodissociation spectra did not correlate as well with the neutral infrared spectrum as did that for perfluoro propylene. The major difference between the neutral infrared spectrum and the ion photodissociation spectrum is that the latter is broadened by up to 50% and shifted to longer wavelengths by up to 0.1 micron (Thorne and Beauchamp, 1984). Experiments using visible light have also shown a strong relationship between the neutral visible spectrum and the visible photodissociation spectrum (Dunbar, 1984). Thus, one should at least in principle be able to differentiate isomeric ions based on the appearance of their photodissociation spectra.

The infrared multiphoton dissociation spectra of protonated 1,2-ethanediol, 1,2- and 1,3-propanediol, 1,2-, 1,3-, 1,4- and 2,3-butanediol,and 1- and 2-butanol were obtained by measuring the amount of photodissociation as a function of wavelength. For each ion the only observed dissociation pathway corresponded to loss of a water

molecule. The neutral vapor-phase infrared spectra for 1,3-propanediol, 1,4- and 2,3-butanediol were obtained and were compared to the corresponding photodissociation spectra.

Certain trends in the photodissociation behavior were observed for diols with related structures. The photodissociation cross section of protonated 1,2-diols increases with increasing length of the attached alkyl chain. For diols with a different number of methylene groups separating the hydroxyl groups, the magnitude of the cross section was observed to alternate between a higher and lower value as a function of chain length. These trends are explained by consideration of the structure and energetics of both reactant and product ions.

Experimental

Ions trapped within the analyzer cell were irradiated with light from the continuous wave CO_2 laser. Irradiation of the ions was achieved by replacing one of the excitation plates with one that contained a 1.5 cm diameter hole covered by a fine Cu mesh (see Figure 2.8). The laser beam was reflected into the cell by a highly polished stainless steel plate that was spot welded to the excitation plate. The laser arrangement is shown in Figure 2.9.

For each point in the photodissociation spectrum the laser was manually tuned to the desired wavelength and the power was adjusted to the same constant value. The laser was turned on and off by a programmable gating pulse from the mass spectrometer data system. For each

photodissociation measurement the laser was gated on and the ions irradiated for 300 ms.

Ions were formed during a 5 ms period by collisions of neutrals with a beam of electrons accelerated to 50 eV. The electron impact fragments were allowed to react for 800 ms with the background neutrals. The major ion/molecule reaction pathway resulted in the formation of the protonated molecule. After this reaction time all ions other than the protonated molecules were removed by a swept frequency ejection pulse (5 ms duration) which excited the unwanted ions to sufficiently large radii that they struck the cell walls and were neutralized. An additional 300 ms period was included during which the ions could be irradiated before detection of the mass spectrum.

Following this last 300 ms time period, the ion signal was measured by recording the ion's mass spectral peak area. Three separate measurements were recorded under conditions of no irradiation, irradiation, and no irradiation to assess the amount of photodissociation. First, a mass spectrum with no laser irradiation was recorded to serve as the reference signal, I_o, and then a second mass spectrum with laser irradiation was recorded to determine I, the ion signal after the irradiation period. To help correct for drift in the ion signal resulting from small pressure or temperature variations during the data acquisition process, a second reference mass spectrum was obtained after irradiation. The value taken for I_o was the average of the first and second reference. The laser was then tuned to a

new wavelength and the above process was repeated. Ion/molecule reactions of the photofragment ions were eliminated by constantly ejecting these ions during irradiation.

The neutral vapor-phase infrared spectra were obtained by using a heated gas cell and a Fourier transform infrared spectrometer. The cell consisted of a glass tube containing two vacuum valves for sample introduction and removal. Sodium chloride windows were mounted to the tube and supported with o-ring seals. To remove any background contamination, the cell was evacuated to below 10^{-3} torr and heated to above 200^{o} C. The samples were prepared by several freeze-pump-thaw cycles to remove residual gases. The samples were then warmed to room temperature or slightly above, and the vapor above the liquid was introduced into the evacuated gas cell. The cell was continuously heated to 150^{o} C while inside the infrared spectrometer to prevent condensation of the vapor on the cell walls or windows.

All samples were obtained from commercial sources and sample purity was confirmed by electron impact mass spectrometry. No further sample purification was necessary other than several freeze-pump-thaw cycles to remove noncondensable gasses.

Results and Discussion

For all protonated molecules the only fragmentation pathway observed was loss of a water molecule. The fragmentation pathway was found to be independent of wavelength and

the photodissociation cross section was observed to vary with wavelength. For most cases the spectral fine structure did not show significant features, and differences in peak positions could not clearly allow confirmation of a unique ion structure. However, the overall magnitude of the photodissociation cross section was observed to vary significantly among isomeric ions and reflects unique ion structures. Results for individual molecules will be discussed below.

Ethanediol

Ethanediol has only one possible configuration. It was initially chosen for study since it was one of the smallest ions observed to dissociate. The protonated molecule may well fall into the class of ions described by the "small molecule limit" (Thorne, 1984), meaning that one or more photons must be resonantly absorbed before attaining the "vibrational quasicontinuum" where further photon absorption is easily facilitated. Since the initial resonance absorptions must correspond to a characteristic frequency of the ion, a wavelength dependence for photodissociation was expected and observed experimentally.

The photodissociation spectrum of protonated 1,2-ethanediol is shown in Figure 3.1. One should note that the cross section for the 10.2 to 10.8 micron range is significantly larger than that for the 9.2 to 9.8 micron range, even when considering the extreme ranges of the confidence limits. For this and all following spectra the

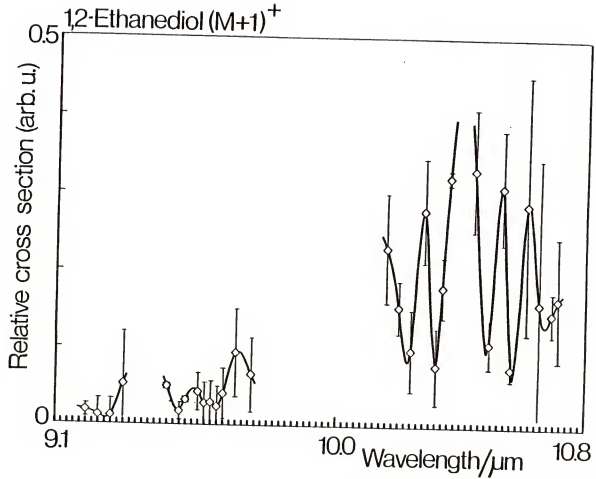

Figure 3.1. Photodissociation spectrum of protonated 1,2-ethanediol over the CO_2 laser spectral range. Ions exposed to 300 ms irradiation at 3.5 watts/cm^2. Bold line is a quadratic spline fit.

data values are the average of at least three independent determinations and the confidence limits are derived from Student's 95% confidence intervals (Young, 1962). The amount of photodissociation was measured at a particular wavelength. The laser was tuned to a new wavelength and the process was repeated. The values obtained from at least three such wavelength "scans" were averaged and used to obtain the confidence limits. The broken portions of the curves where no data were taken reflect the rather limited wavelength range of the CO_2 laser. The CO_2 laser wavelength regions are slightly wider than would be surmised by viewing the spectra, but in order to keep the laser power constant the weaker laser lines were omitted. The solid lines connecting the points are calculated from a computer generated quadratic spline fit. These "artificial" peaks and valleys may or may not correspond to real vibrational fine structure, but the fit is merely included to aid the reader when viewing the spectra.

Propanediols

The photodissociation spectra for protonated 1,2- and 1,3-propane are shown in Figures 3.2 and 3.3, respectively. Note that the photodissociation spectra for these two isomers are clearly distinct from each other based on the relative magnitude of the photodissociation cross section. The relative cross section for the ion obtained from 1,2-propanediol is approximately five times as large as that observed for the protonated molecule of 1,3-propanediol.

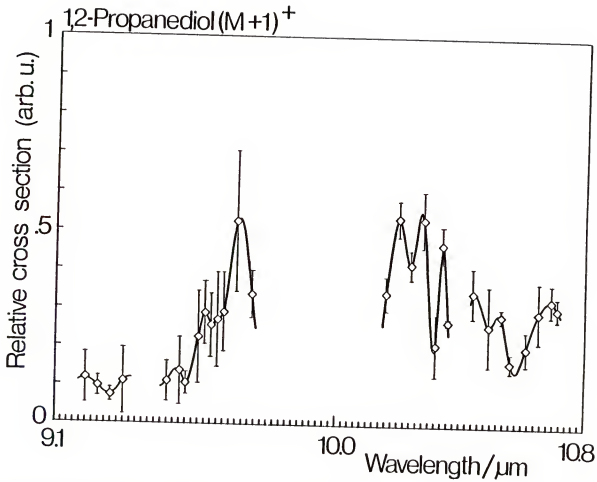

Figure 3.2. Photodissociation spectrum of protonated 1,2-propanediol over the CO_2 laser spectral range. Ions exposed to 300 ms irradiation at 3.5 watts/cm^2. Bold line is a quadratic spline fit.

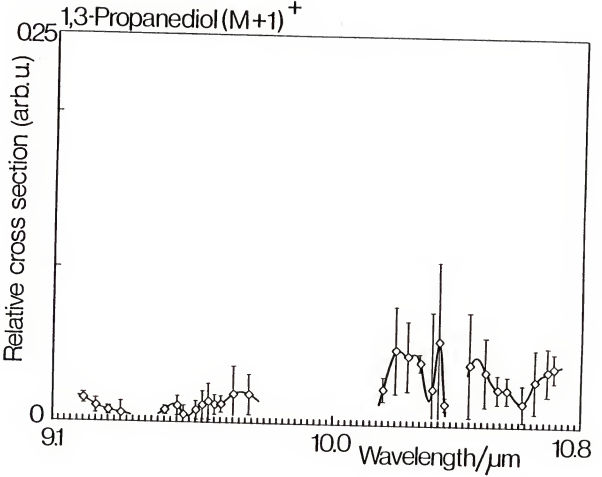

Figure 3.3. Photodissociation spectrum of protonated 1,3-propanediol over the CO_2 laser spectral range. Ions exposed to 300 ms irradiation at 3.5 watts/cm^2. Bold line is a quadratic spline fit.

One reasonable explanation is that upon dissociation the 1,2- isomer forms a more stable secondary carbocation while the 1,3- isomer is limited to the production of a primary carbocation. Thermochemical calculations show that protonated secondary alcohols require less energy to cleave the C-O bond to produce a water molecule and hydrocarbon ion. Protonated 1-propanol, for instance, requires about 35 kcal/mol to lose water, while 2-propanol requires only 24 kcal/mol. The activation energy barrier leading to dissociation, not the enthalpy difference between reactants and products, influences the reaction cross section. However, the activation barrier which leads to the more stable secondary carbocation is expected to be lower.

Butanediols

The photodissociation spectra for 1,2-, 1,3-, 1,4- and 2,3-butanediols are shown in Figures 3.4-3.7. Using the previouly presented argument presented to explain the relative magnitude of the propanediol's cross section, one would predict that the 2,3- isomer would have the largest overall cross section. In order of decreasing cross section the trend would follow,

$$2,3- > 1,2- = 1,3- > 1,4-$$

where the 1,2- and 1,3- isomers have similar cross sections and the 1,4- isomer has the smallest. Instead it was observed that the experimentally determined values follow the order,

$$2,3- = 1,2- > 1,3- = 1,4-.$$

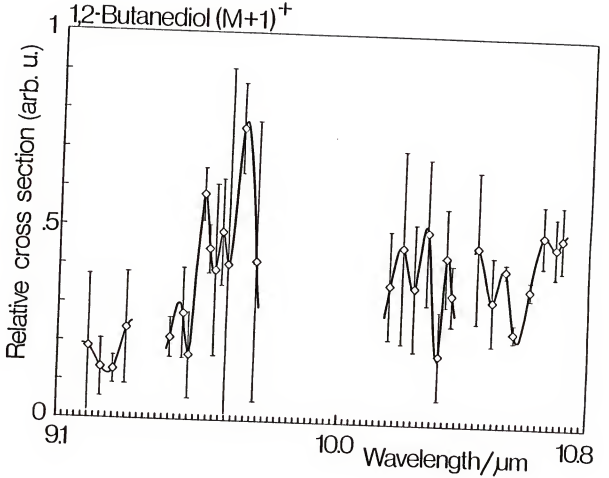

Figure 3.4. Photodissociation spectrum of protonated 1,2-butanediol over the CO_2 laser spectral range. Ions exposed to 300 ms irradiation at 3.5 watts/cm^2. Bold line is a quadratic spline fit.

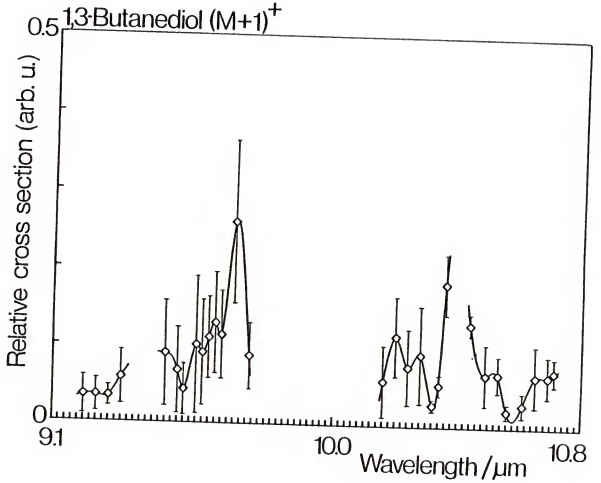

Figure 3.5. Photodissociation spectrum of protonated 1,3-butanediol over the CO_2 laser spectral range. Ions exposed to 300 ms irradiation at 3.5 watts/cm^2. Bold line is a quadratic spline fit.

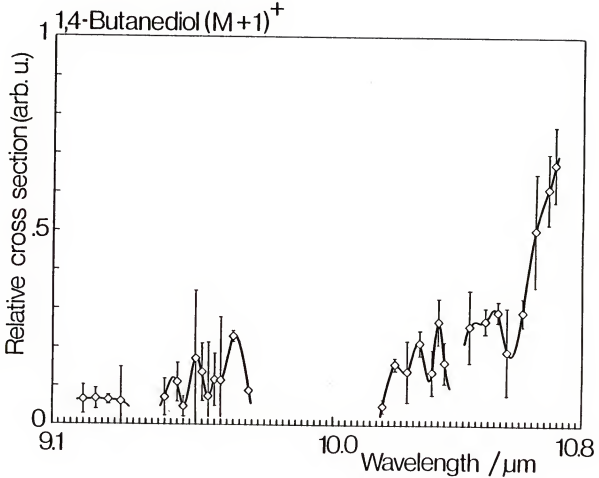

Figure 3.6. Photodissociation spectrum of protonated 1,4-butanediol over the CO_2 laser spectral range. Ions exposed to 300 ms irradiation at 3.5 watts/cm^2. Bold line is a quadratic spline fit.

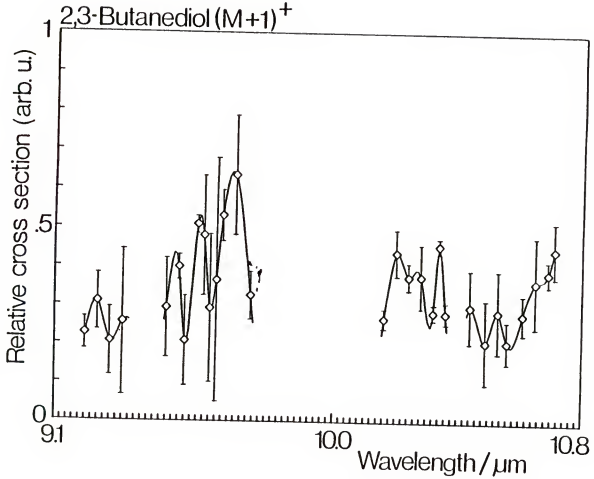

Figure 3.7. Photodissociation spectrum of protonated 2,3-butanediol over the CO_2 laser spectral range. Ions exposed to 300 ms irradiation at 3.5 watts/cm^2. Bold line is a quadratic spline fit.

Clearly, other factors influence the photodissociation cross section than the formation of more stable products. One other possible factor is the formation of stable intramolecular hydrogen bonds, where the proton is shared between two hydroxyl groups. For such cases the activation barrier leading to dissociation increases, since a hydrogen bond must be cleaved before the dissociation process can occur. Another factor that can influence the height of the activation barrier is the neighboring group effect (March, 1977).

To determine the influence of the formation of a primary or secondary carbocation on the photodissociation cross section, the photodissociation spectra for protonated 1- and 2-butanol were obtained. The spectra for these two ions are given in Figures 3.8 and 3.9, respectively. In the 10 micron range 2-butanol was observed to have approximately twice the cross section of 1-butanol. Again, thermochemical calculations show that the primary alcohol (33 kcal/mol) requires more energy to produce $C_4H_9^+$ and a water molecule than the secondary alcohol (21 kcal/mol). The large difference in cross section for the diols (such as the factor of five in the cases of 1,2- and 1,3-propanediol) demonstrates that other factors as well as thermochemistry influence the amount of photodissociation.

The greatest difference in appearance for the butanediols' photodissociation spectra occurs for 1,4- and 2,3-butanediol. For these two compounds the neutral vapor phase infrared spectra were obtained and are shown in

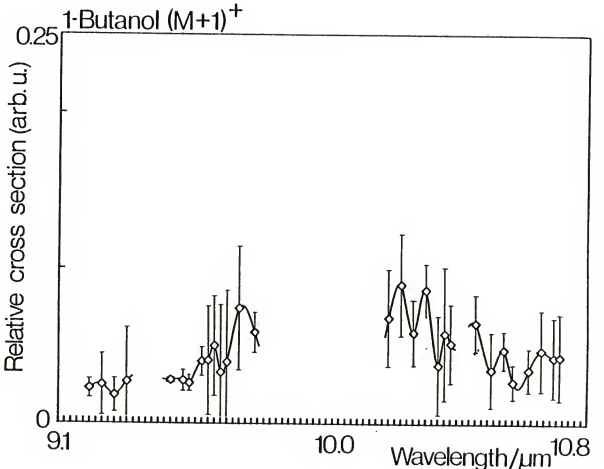

Figure 3.8. Photodissociation spectrum of protonated 1-butanol over the CO_2 laser spectral range. Ions exposed to 300 ms irradiation at 3.5 watts/cm^2. Bold line is a quadratic spline fit.

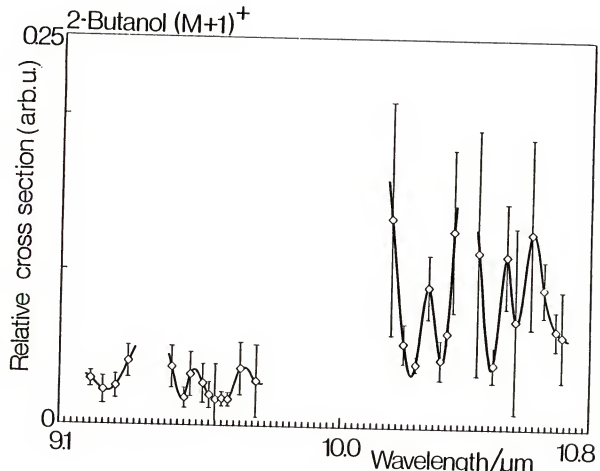

Figure 3.9. Photodissociation spectrum of protonated 2-butanol over the CO_2 laser spectral range. Ions exposed to 300 ms irradiation at 3.5 watts/cm^2. Bold line is a quadratic spline fit.

Figures 3.10 and 3.11. The neutral spectra appear almost identical over this narrow wavelength range, which primarily corresponds to the C-O stretching frequencies. The infrared spectra are of lower resolution due to the inherent limitation of the infrared spectrometer used and pressure broadening of the signal from the relatively high vapor pressures of the samples (relative to the low pressures necessary inside the mass spectrometer). One obvious difference is the apparent absorption increase of the ion relative to the neutral in the 10.2 to 10.8 micron region. The intensity differences could result from changes in bond strength and distortion of the normal modes upon protonation.

The spectral fine structure for both the neutral infrared and photodissociation spectra were not observed to differ significantly. This partly results from the limited wavelength range of the CO_2 laser, 9-11 microns. However, even though the qualitative appearance of the photodissociation spectra is similar, the magnitude of the relative photodissociation cross sections varies widely reflecting differences in ion structure.

Relationships Between Photodissociation Cross Section and Ion Structure

The magnitude of the photodissociation cross section for the 1,2-diols (1,2-ethanediol, 1,2-propanediol, and 1,2-butanediol) was observed to increase as a function of alkyl chain length. This trend is illustrated by Figure 3.12 which shows an increase in the relative cross section

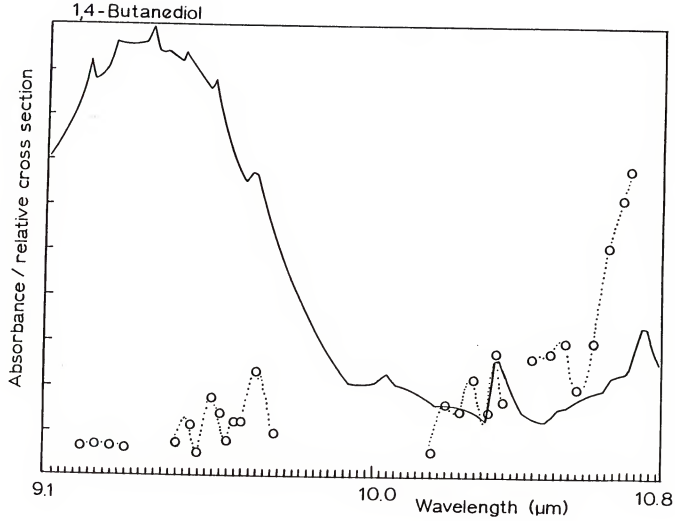

Figure 3.10. Infrared absorption spectrum of 1,4-butanediol at 150° C in 10 cm length cell; (o) - photodissociation spectrum of protonated molecule.

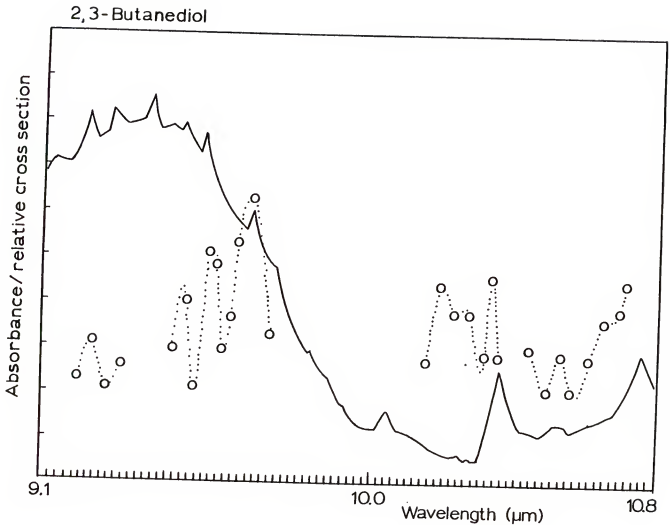

Figure 3.11. Infrared absorption spectrum of 2,3-butanediol at 150° C in 10 c length cell; (o) - photodissociation spectrum of protonated molecule.

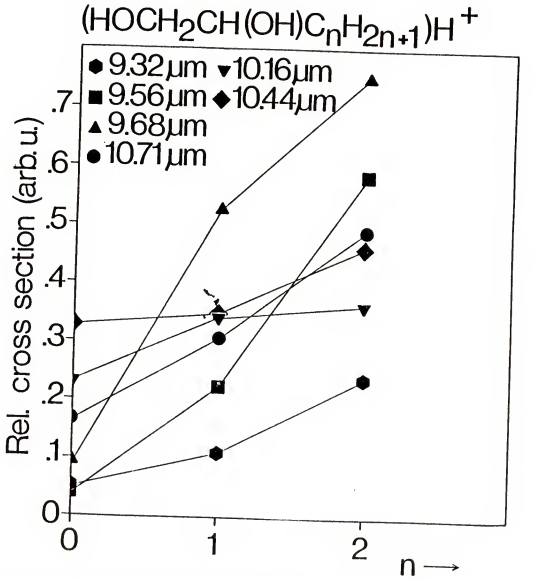

Figure 3.12. Influence of additional alkyl chain length on the relative photodissociation cross section.

for a number of wavelengths as the alkyl chain becomes longer. This increase in cross section is attributed to an increase in the density of states as the molecules become larger and more complex. The vibrational quasicontinuum is more easily accessible for the larger molecules; hence, the rate of dissociation increases and any bottleneck effect for the smaller ions imposed by resonant photon absorption is lessened.

For protonated molecules with increasing methylene groups between the hydroxyl groups (, -dihydroxyalkanes), an interesting oscillation in the photodissociation cross section was observed. This phenomenon is illustrated by Figure 3.13. Here the cross section for chains with an even number of intervening methylene groups is observed to be higher than for those with an odd number. The origin of this phenomenon is not completely understood, but one of the most likely explanations is that at least two different effects with opposing trends are influencing the magnitude of the absorption cross section (vide infra).

Protonated dialcohols tend to form intramolecular hydrogen bonds (Meot-Ner, 1983). A stable intramolecular "bridge" may well decrease the photodissociation cross section since more energy is required to break the proton bond in addition to the C-O bond. Protonated 1,2- diols (or in general, n, n+1-diols) may form intramolecular proton bonds resulting in a cyclic-five membered ring where the proton is one of the ring members. However, a more stable six-membered ring structure could be formed in a 1,3-diol

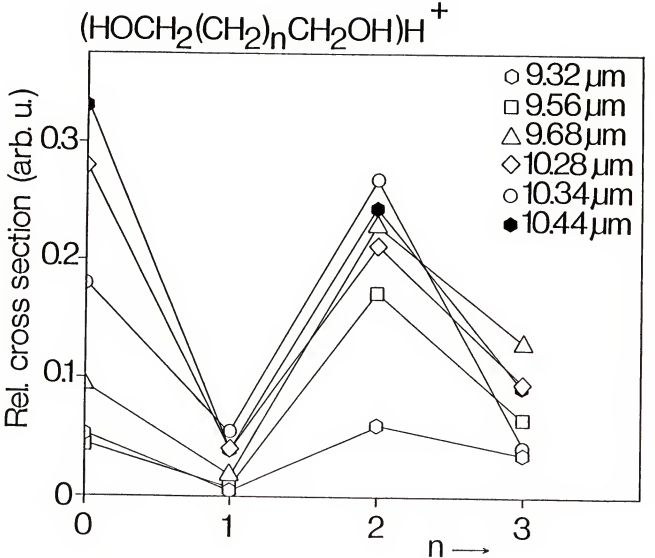

Figure 3.13. Influence of hydroxyl group seperation on the relative photodissociation cross section.

(n, n+2-diol). Compare, for example, the photodissociation spectra of 1,2- and 1,3-butanediol (Figures 3.4 and 3.5).

On the other hand, increasing the number of methylene groups has a different effect. It increases the number of degrees of freedom as the molecule becomes larger, which in turn, lowers the onset of the vibrational quasicontinuum, thus facilitating the sequential absorption of photons. This tends to lower the photodissociation cross section. Other factors, such as the formation of cyclic products or intermediates may also affect the cross section. The net result of these trends is that the magnitude of relative photodissociation "zigzags" up and down as the number of intervening methylene groups increases.

CHAPTER 4
DIFFERENTIATION OF ISOMERIC ION STRUCTURES BY OBSERVATION OF DIFFERENT PHOTOFRAGMENTS

In the preceding chapter infrared multiphoton dissociation wavelength dependence was used to achieve isomeric differentiation for a series of diol isomers. The same photodissociation pathway, loss of water, was observed for each ion. This chapter presents another method of isomeric differentiation using infrared multiphoton dissociation. For the isomeric ions studied, unique photodissociation pathways were observed for ions of different structure. For the work reported below, a number of oxygen-containing ions were chosen, in part because earlier reports (Bomse et al., 1978; Thorne and Beauchamp, 1984) had predicted a high probability that these compounds would absorb CO_2 laser radiation in the 10.6 micron wavelength range, presumably due to excitation of a C-O asymmetric stretching mode in the ions as reported in the preceding chapter. The infrared multiphoton dissociation of two gaseous ions, $C_4H_9O_2^+$ (m/z 89) and $C_5H_{11}O_2^+$ (m/z 103), formed from several ethers and esters, has been studied (vide infra), and quite different dissociation pathways dependent on the ionic precursor have been observed. The photodissociation behavior of four distinct $C_4H_9O_2^+$ isomers is presented in some detail, with limited results for $C_5H_{11}O_2^+$ used to corroborate

dissociation pathways suggested for the smaller ion. Explanation of the different photodissociation pathways is presented in terms of different lowest activation energy dissociation channels for structural isomers. Implications of this controlled means of dissociating ions of moderate to large molecular weight are also discussed.

Experimental Section

All experiments were carried out with a Nicolet FT/MS-1000 Fourier transform mass spectrometer equipped with a 3 tesla superconducting magnet. The cubic ion cyclotron resonance cell (2.54 cm) was modified to allow irradiation of trapped ions by replacing the stainless steel trapping plate through which the electron beam exited the cell with one containing a 1.34 cm diameter hole covered by a copper mesh of approximately 80% transparency, as shown in Figure 2.6. Positive ions were produced by electron impact (EI) (ionizing energies ranged from 9.2 to 50 eV) and trapped in the cell by the magnetic field and an electric trapping field produced by a +1 volt potential applied to the trapping plates. Ion irradiation was carried out with an Apollo Model 570 CW tunable CO_2 laser gated by a trigger pulse from the FTMS instrument which could be chosen to coincide with any pulse in the experimental sequence under software control.

As shown in Figure 2.7, the laser beam was reflected by a NaCl beam splitter and an Au mirror into a spectrum analyzer (Optical Engineering Model 16-A) for wavelength

determination. The main beam was split again by another NaCl beam splitter for power measurement with a Coherent Radiation Model 410 power meter. These two beam splitters were removed during actual ion irradiation. Finally, the main laser beam was reflected by using two gold mirrors into the vacuum chamber of the mass spectrometer, passing through a NaCl window sealed to a vacuum flange with viton O-rings. The flange was at the end of a 1.27 cm diameter stainless steel tube which was inserted into the vacuum chamber through the solid sample inlet system. Before passing through the mesh on the trapping plate (Figure 2.6) the laser beam passed through another mesh of ca. 50% transparency which was used as the electron collector of the ion cyclotron resonance cell. The IR laser beam was aligned with use of a He-Ne laser whose beam was reflected by an Ag mirror and the first beam splitter into the path of the CO_2 laser (Figure 2.7).

Although a wavelength-dependence for multiphoton dissociation of lower molecular weight ions as well as some of those studied here has been observed (see Chapter 3), for these studies a fixed wavelength of 10.6 microns was used with CW power levels of 25-50 watts. Following formation by electron impact or ion/molecule reactions, the ion of interest was typically subjected to laser irradiation for 500 ms. The effect of the mirrors, window, and the meshes described above was to reduce the actual laser power entering the cell by approximately a factor of 10 (to ca.

2.5-5 watts in a beam of ca. 1 cm^2 cross section). Since the cell interior consists of highly polished stainless steel, the laser beam was reflected from the trapping plate opposite the one through which it entered the cell. This reflection effectively doubled the laser irradiance to a value of 5-10 W/cm^2. Under these conditions photodissociation rate constants of ca. 10 s^{-1} were observed.

Pressures of neutrals from which the ions were formed were maintained in the 2-5 X 10^{-8} torr range as measured on an ionization gauge. These pressure were sufficiently high to produce adequate ion intensities but low enough that reactions of photo-produced ions to reform their parents were relatively slow (vide infra). For CID experiments Ar was added as a collision gas to a total pressure of 1-2 x 10^{-6} torr.

In order to avoid interference which might arise from either competing ion-molecule formation reactions or competing multiphoton dissociation pathways, photodissociation of an ion was carried out after ejection from the cell of all ions except the one under study. Many of the ions of interest were formed as products in ion/molecule reactions, and for these ions an additional reaction time, usually 500 ms, was added to the experimental sequence before ion selection and irradiation. Since reactive ions can undergo ion/molecule reactions during the laser irradiation period, all spectra were taken both with and without laser irradiation with the same pulse sequence.

In some cases the photofragment ions reacted with neutral molecules present in the system to reform the photodissociating ion. These back reactions complicated the study of the photodissociation effect and made it difficult to observe the actual extent of photodissociation. In order to eliminate this problem, the photofragment ion was continually ejected during the laser irradiation period and the extent of photodissociation was determined from the decrease of the parent peak. An example of this effect for the $C_5H_{11}O_2^+$ ion formed from propyl acetate is shown in Figure 4.1. Figure 4.1a shows the mass spectrum after ejection of all ions but m/z 103 ($C_5H_{11}O_2^+$), and the mass spectrum following 500 ms of laser irradiation is shown in Figure 4.1b. When the m/z 61 photofragment ion was continually ejected from the cell during laser irradiation, the mass spectrum shown in Figure 4.1c was obtained. In this case, the m/z 61 ions were unable to react with propyl acetate to reform the $C_5H_{11}O_2^+$ ion and virtually 100% photodissociation of the latter ion was observed; hence photodissociation was markedly more effective than might be surmised from Figure 4.1b.

All of the compounds used were commercially available analytical grade chemicals. All compounds were additionally purified by several freeze-pump-thaw cycles before introduction into the mass spectrometer. No significant level of any impurity was detected by standard FTMS wide-range mass analysis prior to laser irradiation experiments.

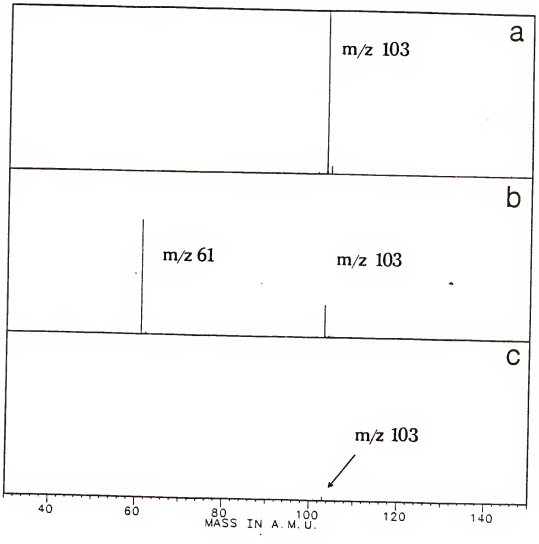

Figure 4.1. Photodissociation of protonated propyl acetate ($C_5H_{11}O_2^+$) with (a) laser off, (b) laser on for 500 ms, (c) and m/z 61 photoproduct ejected during irradiation (ordinate is ion intensity).

Results and Discussion

Differing photodissociation pathways for ions of the same mass-to-charge ratio formed from different precursors have been observed in this work. Such an observation strongly suggests that isomeric ions are being formed and differentiated by infrared multiphoton dissociation. The long time scales of our experiments (ca. 1 s for ion formation, irradiation, and detection) help to ensure that only stable, long-lived isomers are being studied. All observed dissociations were checked at both high (50 eV) and low (vide infra) electron energies to assess the effect on the photodissociation process of excess internal energy in the ions prior to photodissociation. The absence of any observed effect indicated that different dissociation pathways were not caused merely by differing internal energy in ions of the same structure.

The photodissociation pathways observed for each ionic system can be used as guides to the probable structure of the ions prior to photodissociation. Thermochemical data are not available for several of the postulated isomeric structures, so the energetics of most of the pathways observed cannot be calculated. Nonetheless, with use of those data which are available, it appears that dissociation pathways of lowest activation energy (which are observed in MPD) correspond to those of lowest calculated endoergicity (Thorne and Beauchamp, 1984). As indicated in the following discussion, quite reasonable choices for ion structures and

lowest energy dissociation are in excellent agreement with experimental results.

$C_4H_9O_2^+$: Photodissociation of this ion (m/z 89) as produced from seven different precursors was studied. In each case reactions which produce the m/z 89 ion are reported and discussed, followed by the photodissociation behavior.

1,4-Dioxane. In this system $C_4H_9O_2^+$ is formed by proton-transfer reactions to the dioxane molecule. For example, the molecular ion of dioxane undergoes a reaction with neutral dioxane:

$$C_4H_8O_2^+ + C_4H_8O_2 \rightarrow C_4H_9O_2^+ + C_4H_7O_2 \qquad (4.1)$$

The electron impact induced fragment $C_2H_5O^+$ also reacts with the parent molecule and produces protonated dioxane:

$$C_2H_5O^+ + C_4H_8O_2^+ \rightarrow C_4H_9O_2^+ + C_2H_4O \qquad (4.2)$$

The neutral molecule produced in reaction 4.2 may be acetaldehyde (although the identity of neutrals cannot be established in the ICR technique). The ion $C_2H_5O^+$, in addition to being produced by electron impact ionization, is formed by an ion/molecule reaction involving the molecular ion:

$$C_4H_8O_2^+ + C_4H_8O_2 \rightarrow C_2H_5O^+ + (C_6H_{11}O_3) \qquad (4.3)$$

Thus production of $C_4H_9O_2^+$ also occurs via the consecutive reaction system $C_4H_8O_2^+ \rightarrow C_2H_5O^+ \rightarrow C_4H_9O_2^+$.

Irradiation of protonated dioxane by the CO_2 laser tuned to a wavelength of 10.6 microns leads to photodissociation of the ion, producing $C_2H_5O^+$:

$$C_4H_9O_2^+ + nhv \longrightarrow C_2H_5O^+ + C_2H_4O \qquad (I)$$

(see Figure 4.2a).

Most studies were carried out on ions formed with 50 eV ionizing electron energy. To lessen the chances of significant internal excitation in primary and product ions, the electron energy was reduced to 11 eV and photodissociation of the protonated dioxane was again studied. Under these conditions, all ions except the parent ion, $C_4H_8O_2^+$, were ejected from the cell and $C_4H_9O_2^+$ was produced exclusively by reaction 4.1. Only process I was observed. Since the photodissociation product $C_2H_5O^+$ is also a precursor of $C_4H_9O_2^+$ (reaction 4.2), it reacts with dioxane as soon as it is produced by photodissociation to reform protonated dioxane. To avoid complication due to this process, $C_2H_5O^+$ was continuously ejected from the analyzer cell during the laser irradiation period in experiments where the extent of dissociation was determined.

The m/z 89 ion formed via reactions 4.1 and 4.2 might retain the cyclic neutral structure upon protonation, with a proton located either on one of the oxygens or alternatively between the two oxygens in a "boat" conformation of the dioxane. Such a cyclic $C_4H_9O_2^+$ structure requires cleavage of two bonds during photodissociation, since $C_2H_5O^+$ is observed as the dissociation product. The first cleavage

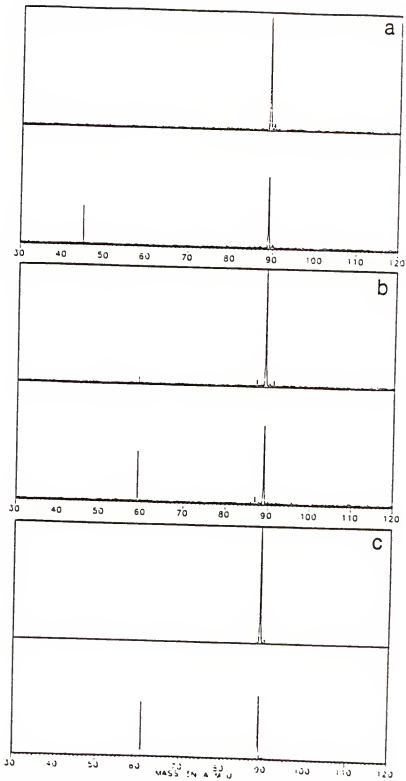

Figure 4.2. Photodissociation of $C_4H_9O_2^+$ m/z 89 from 3 precursors: (a) photoproduction of $C_2H_5O^+$ from protonated 1,4-dioxane; (b) photoproduction of $C_3H_7O^+$ from the $C_4H_9O_2^+$ fragment ion in bis(2-methoxyethyl) ether; (c) photoproduction of $C_2H_5O_2^+$ from protonated ethyl acetate. (Upper spectrum is laser off; lower is laser on.)

would produce a ring-opened ion of the same mass as the cyclic one and the second step would involve cleavage of a carbon-oxygen bond with loss of acetaldehyde most probable (see Figure 4.3a). On the other hand, protonation of dioxane might impart sufficient internal energy to open the ring, with photodissociation then proceeding via the second half of the pathway shown in Figure 4.3a (see Figure 4.3b).

In the following discussion, each proposed isomeric structure will be labeled by a lower case letter, and the photodissociation scheme postulated for that isomer will be labeled with the same upper case letter.

A three-membered ring intermediate ion formed by neighboring group participation (March, 1977) is also possible during the photodissociation process, in which case the mechanism is shown in Figure 4.3c. Further evidence supporting structure a and its dissociation via Scheme A is obtained by studying the subsequent behavior of the m/z 45 ion produced in this photodissociation. After its formation during laser irradiation, this ion reacts completely with dioxane via proton transfer. Such behavior is characteristic (Beauchamp and Dunbar, 1970) of the most stable (Keyes and Harrison, 1974; Bowen et al., 1977; Nobes et al., 1981) m/z 45 isomer, protonated acetaldehyde, shown in Scheme A.

2-(2-Ethoxyethoxy)ethanol. A $C_4H_9O_2^+$ ion is also produced from 2-(2-ethoxyethoxy)ethanol, mainly as a

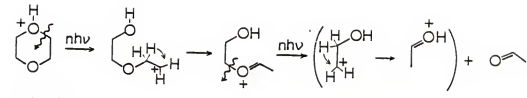

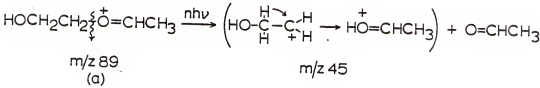

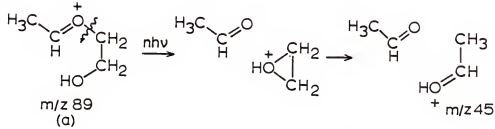

Figure 4.3. (a) top equation: possible photodissociation pathway for "cyclic" $C_4H_9O_2^+$, (b) middle equation: photodissociation Scheme A, (c) botton equation: possible photodissociation pathway for "linear" $C_4H_9O_2^+$.

reaction product of the major fragment ion, $C_2H_5O^+$:

$$C_2H_5O^+ + C_6H_{14}O_3 \longrightarrow C_4H_9O_2^+ + C_4H_{10}O_2 \qquad (4.4)$$

The same photodissociation process was observed for this ion as for the m/z 89 ion produced from 1,4-dioxane, namely process I above. Considering the formation of the ion via reaction 4, the structure a which dissociates via Scheme A would again be expected. Again, in this system photoproduced m/z 45 ions react (see Figure 4.4) completely to protonate the parent neutral, indicating a protonated acetaldehyde structure for these photofragment ions and supporting structure a as the best assignment for the $C_4H_9O_2^+$ isomer undergoing photodissociation.

Bis(2-methoxyethyl) ether (diglyme). A $C_4H_9O_2^+$ fragment ion is produced by electron impact ionization of diglyme. After ejection of all other ions, irradiation of this ion results in photofragmentation, producing $C_3H_7O^+$, m/z 59:

$$C_4H_9O_2^+ + nhv \longrightarrow C_3H_7O^+ + CH_2O \qquad (II)$$

(see Figure 4.2b). Experiments at an electron energy of 10 eV, slightly above the m/z 89 ion's appearance potential, gave the same results as those seen with 50 eV ionizing energy.

The EI-induced fragmentation of diglyme cleaves a carbon-carbon bond and causes loss of CH_2OCH_3 as the neutral species (see Figure 4.5a). Thus, the resultant $C_4H_9O_2^+$ most likely has a methylene and not a hydroxyl group at the end of a linear ion. The photodissociation process then

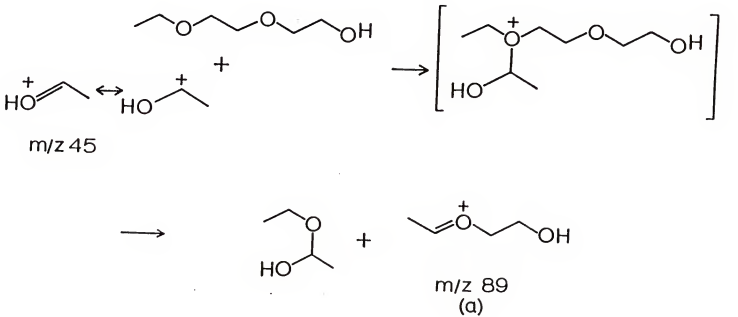

Figure 4.4. Ion molecule reaction of $C_2H_5O^+$ with 2-(2-ethoxyethoxy) ethanol producing $C_4H_9O_2^+$.

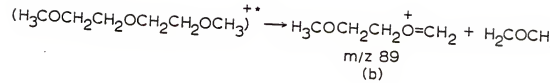

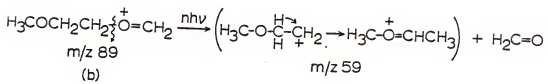

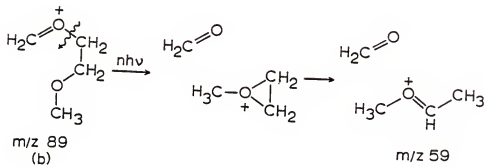

Figure 4.5. (a) top equation: electron impact ionization of diglyme produce $C_4H_9O_2^+$, (b) middle equation: photodissociation Scheme B, (c) bottom equation: possible photodissociation pathway of $C_4H_9O_2^+$ (m/z 89) producing $C_3H_7O^+$ (m/z 59).

involves cleavage of a carbon-oxygen bond and a neutral formaldehyde molecule is apparently lost (see Figure 4.5b). Again invoking neighboring group participation, the mechanism can be alternately formulated with a three-membered ring intermediate ion as shown in Figure 4.5c.

1,2-Dimethoxyethane. The electron impact mass spectrum of 1,2-dimethoxyethane contains relatively little $C_4H_9O_2^+$. However, the ion is formed by ion/molecule reactions, primarily from $C_2H_5O^+$, which is a major fragment ion in the mass spectrum:

$$C_2H_5O^+ + C_4H_{10}O_2 \rightarrow C_4H_9O_2^+ + C_2H_6O \qquad (4.5)$$

Thus it appears that $C_2H_5O^+$ forms dimethyl ether by a hydride transfer reaction involving the 1,2-dimethoxyethane neutral. Hydride transfer is a characteristic reaction (Beauchamp and Dunbar, 1970) of the methoxymethyl cation isomeric form of m/z 45.

Photodissociation of this $C_4H_9O_2^+$ isomer was observed at both high and low electron energies, down to the appearance potential of its $C_2H_5O^+$ precursor. MPD gave rise to the photofragment $C_3H_7O^+$, as shown in process II above. Formation of isomer b, which dissociates via Scheme B, is quite reasonable given its formation via hydride transfer from the parent molecule.

2-Methoxyethanol. A $C_4H_9O_2^+$ ion is formed from 2-methoxyethanol. The fragment ion $C_2H_5O^+$ produces $C_4H_9O_2^+$ by a reaction with the neutral,

$$C_2H_5O^+ + C_3H_8O_2 \text{ --> } C_4H_9O_2^+ + CH_4O \qquad (4.6)$$

or by two consecutive reactions via $C_3H_7O^+$:

$$C_2H_5O^+ + C_3H_8O_2 \text{ --> } C_3H_7O^+ + C_2H_6O_2 \qquad (4.7)$$

$$C_3H_7O^+ + C_3H_8O_2 \text{ --> } C_4H_9O_2^+ + C_2H_6O \qquad (4.8)$$

Multiphoton dissociation of this $C_4H_9O_2^+$ ion yields $C_3H_7O^+$ as shown in process II above. This photodissociation was studied at low electron energies (11 eV) after ejection of all ions but $C_2H_5O^+$, which then formed $C_4H_9O_2^+$, and it still proceeded as shown in (II). Reaction 6 most likely involves elimination of methanol, as shown in Figure 4.6a.

The photodissociation then proceeds as shown in Scheme B. Observation of this photodissociation pathway gives strong evidence for a $C_4H_9O_2^+$ ion with no terminal OH but rather two etheric oxygens in the central portion of the chain. Such a structure would result from reaction of the less stable methoxymethyl cation, known (Beauchamp and Dunbar, 1970) to form in etheric systems. Reaction of the more stable protonated acetaldehyde m/z 45 isomer with 2-methoxyethanol would lead to $C_4H_9O_2^+$ with a terminal OH, as in the case of dioxane and 2-(2-ethoxyethoxy)ethanol. Those ions, however, photodissociate to form $C_2H_5O^+$ rather than $C_3H_7O^+$.

Formation of the m/z 89 ion via reaction 8, with probable loss of ethanol, can proceed as shown in Figure 4.6b. The $C_4H_9O_2^+$ ion would again be predicted to photodissociate as shown in Scheme B.

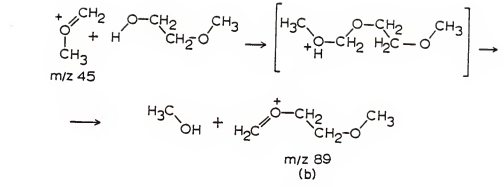

Figure 4.6a. Ion molecule reaction of $C_2H_5O^+$ (m/z 45) with 2-methoxyethanol producing $C_4H_9O_2^+$ (m/z 89).

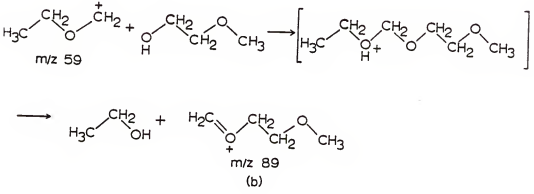

Figure 4.6b. Ion molecule reaction of $C_3H_7O^+$ (m/z 59) with 2-methoxyethanol producing $C_4H_9O_2^+$ (m/z 89).

Ethyl Acetate. Protonated ethyl acetate also possesses the formula $C_4H_9O_2^+$. Protonation occurs via reaction of the fragment ions $C_2H_3O^+$, $C_2H_5O^+$, $C_2H_5O_2^+$, and $C_4H_6O^+$ with the neutral molecule:

$$C_2H_3O^+ + C_4H_8O_2 \rightarrow C_4H_9O_2^+ + C_2H_2O \quad (4.9)$$

$$C_2H_5O^+ + C_4H_8O_2^+ \rightarrow C_4H_9O_2^+ + C_2H_4O \quad (4.10)$$

$$C_2H_5O_2^+ + C_4H_8O_2 \rightarrow C_4H_9O_2^+ + C_2H_4O_2 \quad (4.11)$$

$$C_4H_6O^+ + C_4H_8O_2 \rightarrow C_4H_9O_2^+ + C_4H_5O \quad (4.12)$$

The fragments $C_4H_6O^+$, $C_2H_5O^+$, and $C_2H_5O_2^+$ also contribute to formation of $C_4H_9O_2^+$ by producing $C_2H_3O^+$ in ion-molecule reactions, which are then followed by reaction 9.

Photodissociation of $C_4H_9O_2^+$ ions formed by reactions 9-12 was studied at electron impact energies of 50 and 11 eV. Photodissociation with a similar cross section was observed for both electron energies, leading to $C_2H_5O_2^+$:

$$C_4H_9O_2^+ + nhv \rightarrow C_2H_5O_2^+ + C_2H_4 \quad (III)$$

(see Figure 4.2c). Again the extent of photodissociation was more easily studied by ejecting the photofragment $C_2H_5O_2^+$ during the laser irradiation time, since it reacted to reform $C_4H_9O_2^+$ as shown in reaction 11. Photofragmentabtion consistent with a McLafferty-type rearrangement (McLafferty, 1959) best explains the loss of ethylene and formation of an m/z 61 ion in this system (see Figure 4.7).

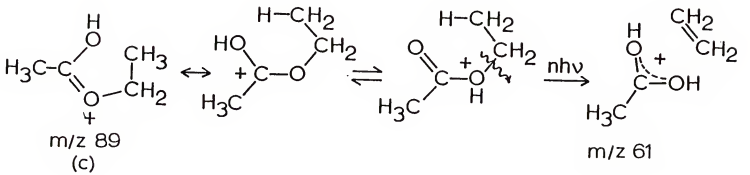

Figure 4.7. Photodissociation Scheme C.

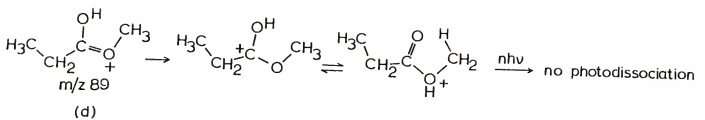

Figure 4.8. Photodissociation Scheme D.

Methyl Propionate. Protonated methyl propionate is obtained primarily by reaction of a fragment ion, $C_3H_5O^+$, with the neutral molecule:

$$C_3H_5O^+ + C_4H_8O_2 \text{ --> } C_4H_9O_2^+ + C_3H_4O \qquad (4.13)$$

This $C_4H_9O_2^+$ isomer exhibited no photodissociation over the range of wavelengths available (see Figure 4.8). The absence of photodissociation in this case is reasonable, since thermochemical calculations (Franklin et al., 1969; Long and Munson, 1973; Rosenstocket al., 1977; Aue and Bowers, 1979) show that abstraction of a CH_2 radical from protonated methyl propionate requires much more energy (103 kcal/mol) than ethylene abstraction from protonated ethyl acetate (30 kcal/mol) shown in Scheme C. An alternate dissociation to give CH_3^+ and propionic acid is probably the lowest energy pathway available to protonated methyl propionate, but it still requires ca. 97 kcal/mol, apparently more than can be supplied in this type of photodissociation process.

$C_5H_{11}O_2^+$. Photodissociation pathways observed for ions of empirical formula $C_5H_{11}O_2^+$ (m/z 103) strengthen conclusions drawn about m/z 89 structural isomers. Two distinct photodissociation pathways were seen for $C_5H_{11}O_2^+$ ions formed from three different precursors.

Bis(2-methoxyethyl) ether (diglyme). In diglyme $C_5H_{11}O_2^+$ is produced as the product of an ion/molecule reaction involving $C_3H_7O^+$:

$$C_3H_7O^+ + C_6H_{14}O_3 \text{ --> } C_5H_{11}O_2^+ + C_4H_{10}O_2 \quad (14)$$

Three different pathways for ion formation can be envisioned: (1) simple C-O bond cleavage in the m/z 193 ion/molecule collision complex; (2) neighboring group participation involving a three-membered ring intermediate; or (3) formation of a six-membered ring intermediate (see Figure 4.9). Multiphoton dissociation of this ion yielded $C_3H_7O^+$:

$$C_5H_{11}O_2^+ + nhv \text{ --> } C_3H_7O^+ + C_2H_4O \quad (IV)$$

The photodissociation process once again involves C-O bond cleavage, perhaps proceeded by ring opening if the ion retains one of the cyclic structures shown above. Scheme E shown in Figure 4.10a is analogous with Scheme B, with an additional methyl group added to the photodissociating ion and subsequent formation of acetaldehyde rather than formaldehyde.

2-Methoxyethanol. The fragment ion $C_3H_7O^+$ reacts with 2-methoxyethanol to produce $C_5H_{11}O_2^+$:

$$C_3H_7O^+ + C_3H_8O_2 \text{ --> } C_5H_{11}O_2^+ + CH_4O \quad (4.15)$$

Addition of $C_3H_7O^+$ to the parent neutral followed by rearrangement and loss of methanol is entirely analogous to reaction 6 (see Figure 4.10b), which involved addition of $C_2H_5O^+$, rearrangement, and loss of methanol. As would be expected, this ion dissociates via C-O bond cleavage to form an m/z 59 ion and acetaldehyde, following Scheme E above.

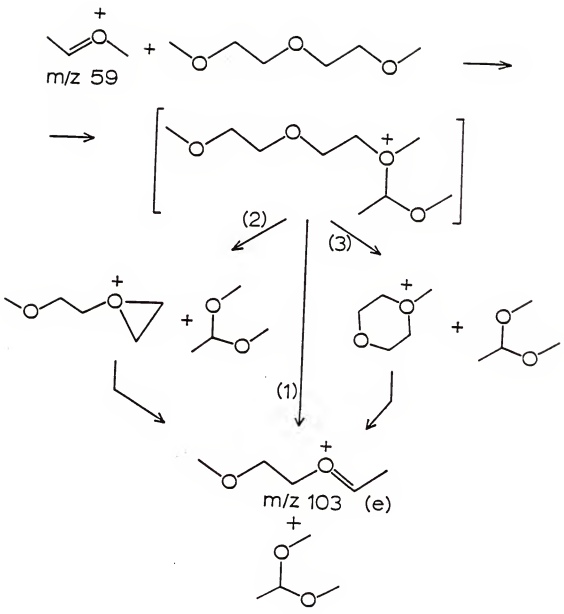

Figure 4.9. Possible ion molecule reaction pathways of $C_3H_7O^+$ with diglyme producing $C_5H_{11}O_2^+$ (m/z 103).

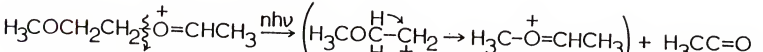

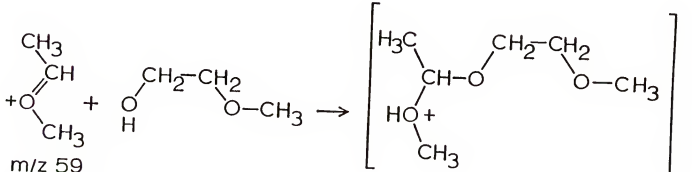

Figure 4.10. (a) top equation is photodissociation scheme E, (b) botton equation is a possible $C_3H_7O^+$ ion molecule reaction pathway producing $C_5H_{11}O_2^+$.

Propyl Acetate. The fragments $C_2H_3O^+$, $C_2H_5O_2^+$, and $C_3H_5O_2^+$ produced a $C_5H_{11}O_2^+$ ion by ion/molecule reactions:

$$C_2H_3O^+ + C_5H_{10}O_2 \rightarrow C_5H_{11}O_2^+ + C_2H_2O \quad (4.16)$$

$$C_2H_5O_2^+ + C_5H_{10}O_2 \rightarrow C_5H_{11}O_2^+ + C_2H_4O \quad (4.17)$$

$$C_3H_5O_2^+ + C_5H_{10}O_2 \rightarrow C_5H_{11}O_2^+ + C_3H_4O_2 \quad (4.18)$$

At 11 eV electron energy the only fragment ion observed is m/z 61, $C_2H_5O_2^+$, which then reacts solely via reaction 17 to produce $C_5H_{11}O_2^+$. An ion/molecule reaction of m/z 43, $C_2H_3O^+$, also produces $C_2H_5O_2^+$, which in turn reacts to form the protonated molecule via reaction 17.

Infrared photodissociation in this case gave

$$C_5H_{11}O_2^+ + nhv \rightarrow C_2H_5O_2^+ + C_3H_6 \quad (V)$$

This photodissociation behavior is best explained by a McLafferty-type rearrangement similar to that shown in Scheme C for protonated ethyl acetate (see Figure 4.11). The products of this photodissociation are most likely protonated acetic acid and a propylene molecule. Thermochemical calculations (Franklin et al., 1969; Long and Munson, 1973; Rosenstock et al., 1977; Aue and Bowers, 1979) show that such a photodissociation requires about the same amount of energy (31 kcal/mol) as ethylene loss from protonated ethyl acetate (30 kcal/mol).

All of the photodissociation pathways observed in this study involved C-O rather than C-C bond cleavages. While either of these bond types requires approximately the same

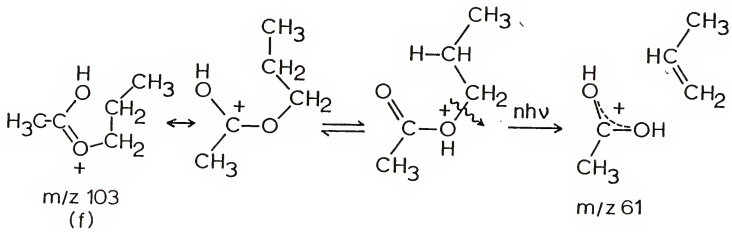

Figure 4.11. Photodissociation Scheme F.

energy for homolytic bond cleavage in neutral species (ca. 80-90 kcal/mol), this equality apparently does not hold true for the ionized, often protonated, oxygen-containing hydrocarbons studied in this work. Heats of formation of the many ions involved in the processes observed are not uniformly available, but sample calculations for smaller ions can be performed. Thus, for example, cleavage of the C-O bond in protonated methyl n-propyl ether to produce methanol and $n\text{-}C_3H_7^+$ requires ca. 14 kcal/mol less energy than cleavage of the C-C bond to form dimethyl ether and $C_2H_5^+$ (Franklin et al., 1969; Long and Munsom, 1973; Rosenstock et al,, 1977; Aue and Bowers, 1979). Formation of formaldehyde and $n\text{-}C_3H_7^+$ by C-O bond cleavage in $CH_3\text{-}CH_2\text{-}CH_2\text{-}O^+\text{=}CH_2$ requires ca. 17 kcal/mol less than formation of 1,2-epoxyethane and $C_2H_5^+$ via C-C bond cleavage (Franklin et al., 1969; Long and Munson, 1973; Rosenstock et al, 1977; Aue and Bowers, 1979). Also protonation of the hydroxyl oxygen on n-propanol lowers the C-O bond strength from 93 to 36 kcal/mol (Franklin et al., 1969; Long and Munson, 1973; Rosenstock et al., 1977; Aue and Bowers, 1979).

Collision-induced dissociation techniques are widely used to obtain structural information about gaseous ions. In these methods, collisions impart a distribution of internal energies to the ions of interest, which can then dissociate, often producing a number of different fragment ions. Multiphoton photodissociation utilizing a CW CO_2 laser was observed to be a more controlled, low-energy

process. For the systems reported here, only one dissociation pathway was seen in IRMPD, corresponding to the fragmentation process of lowest activation energy available to the ion. CID studies have been performed in our FTMS instrument for all of the ions for which multiphoton dissociation was studied and in every case multiple dissociation pathways were seen. Results are presented in Table 4.1. For the ions studied in this work the fragment ion observed in highest abundance after CID corresponded to the only ion produced by multiphoton dissociation. However, for other oxygen- and nitrogen-containing ions this has not always proven to be the case (see Chapter 5). This will be discussed further in the following chapter.

Thus, infrared multiphoton dissociation can complement CID studies by identifying unambiguously the lowest activation energy fragmentation pathway (most often corresponding to the weakest bond) in the ion under study. While the technique described here is limited to those ions which absorb in the 9.2-10.8 micron region, the effect has been observed for many classes of compounds, particularly those containing heteroatoms. Larger ions with sufficient degrees of freedom to guarantee absorption directly into a quasicontinuum should be especially suited for the technique. Since collisions of these ions with typical (much lighter) target gases in CID experiments may not impart sufficient internal energy to cause fragmentation another method to produce fragmentation is needed. Infrared

Table 4.1
Comparison of collision-induced dissociation and inrfared multiphoton dissociation.

Ion	Precursor	m/z of dissociation products: CID (Ar collision gas)	m/z of dissociation products: IRMPD
$C_4H_9O_2^+$ (m/z 89)			
	dioxane	45,29	45
	2-(2-ethoxyethoxy)ethanol	45,73,61	45
	bis(2-methoxyethyl)ether	59,31,29	59
	1,2-dimethoxyethane	59,45,31,29	59
	ethyl acetate	61,43,29,27	61
	methyl propinate	57,45,29,27	
$C_5H_{11}O_2^+$ (m/z 103)			
	bis(2-methoxyethyl)ether	59,31,29	59
	2-methoxyethanol	59,45,31,29	59
	propyl acetate	61,43,27	61

universally applicable. Ion in the m/z 500-700 have been observed to dissociate and these findings are presented in Chapter seven.

Conclusions

The use of Fourier transform ion cyclotron resonance mass spectrometry enhances the study of infrared multiphoton dissociation of gaseous ions. Long ion trapping times are afforded by the high magnetic fields available (3 tesla) and (often multiple) ion ejection can be employed at any time during the experimental sequence to remove complicating reactions or unwanted ions. Differentiation of several $C_4H_9O_2^+$ (m/z 89) and $C_5H_{11}O_2^+$ (m/z 103) ions produced from some oxygen-containing hydrocarbon systems has been demonstrated. A $C_4H_9O_2^+$ ion of structure a (vide ante) is found in p-dioxane and 2-(2-ethoxyethoxy)ethanol, while structure b is produced from bis(2-methoxyethyl)ether, 1,2-dimethoxyethane, and 2-methoxyethanol, structure c results from protonation of ethyl acetate, and structure d results from protonation of methyl propionate. $C_5H_{11}O_2^+$ ions of structure e are formed from bis(2-methoxyethyl) ether and 2-methoxyethanol, and protonation of propyl acetate produces an ion of structure f. Compared to CID, where numerous fragment ions are produced, infrared MPD is a highly efficient (under ideal conditions 100% conversion to fragments was observed), low-energy means of generating usually only one fragment ion. For the ions studied here, the one fragment ion produced by MPD corresponded to the highest intensity ion resulting from CID.

CHAPTER 5
INFRARED MULTIPHOTON DISSOCIATION AND COLLISION-INDUCED DISSOCIATION STUDIES OF SOME GASEOUS ALKYLAMINE IONS

In the studies of the last chapter involving oxygen-containing systems, primarily esters and ethers, the sole fragment produced by infrared multiphoton dissociation (IRMPD) was always the same as the most intense ion observed following collision-induced dissociation (CID). While such behavior would be expected for many ionic systems, it should not hold true in all cases. The relatively slow excitation process in IRMPD experiments leads to dissociation via the channel of lowest activation energy. In CID a range of internal energies is imparted to an ion during the relatively short collision duration; of the resulting fragment ions, the one of highest intensity need not be obtained via the pathway of lowest activation energy. This is particularly to be expected if substantial rearrangement occurs during the fragmentation (i.e., if the entropy of activation is high). Quite significant differences between CID and IRMPD have been observed for alkylamine ions (vide infra); the results of applying the two dissociation techniques to this class of ions are reported here.

The only bond cleavage observed during the earlier IRMPD investigations involved C-O, and not C-C or C-H bonds. Available thermochemical data showed that these were the

weakest bonds in the ions under study. Thus the dissociation of lowest overall endothermicity (corresponding to breaking the weakest bond in the ion) correlated directly with the dissociation pathway with lowest activation energy (observed in IRMPD experiments). Extension of the validity of this behavior to nitrogen-containing was sought, to see if C-N bonds would again cleave preferentially to C-C bonds.

Infrared multiphoton dissociation of triethylamine and benzylamine ions produced by multiphoton ionization has been reported (Haas et al., 1982; Cantanzarite et al., 1983), and metastable ions produced by multiphoton ionization have been compared to those produced with electron impact ionization (Haas and Lifshitz, 1983). One other IRMPD study (Moylan and Brauman, 1982) of the ethylisopropylammonium ion gave useful mechanistic information about the ethylisopropylamine proton-transfer system. The present work reports IRMPD and CID results for molecular, protonated, and fragment ions of various tri- and di- n-propyl-, isopropyl-, and ethylamines. Results for IRMPD and CID of the various alkylamines are discussed in light of the earlier studies (Haas et al., 1982; Cantanzarite et al., 1983; Haas and Lifshitz, 1983; Moylan and Brauman, 1982).

Experimental

Figure 2.9 shows the experimental apparatus used for IRMPD studies. The CO_2 laser beam was reflected from two gold plated glass mirrors through a zinc selenide window into the vacuum system of a modified Nicolet FT/MS-100 mass spectrometer. For monitoring laser power and wavelength, a

mirror supported by a kinematic mount was inserted into the beam path. This reflected the laser beam to a germanium beam splitter which allowed it to be directed to both a power meter and a spectrum analyzer. For the work reported here, a fixed wavelength (10.61 microns) and high output power (ca. 50 W measured at the laser) were used.

The 2.54 cm cubic FTICR analyzer cell was modified by adding a 15-mm diameter hole covered by wire mesh to one transmitter plate (see Figure 2.10). This modification caused no significant deterioration of the ion signal. The actual laser irradiance inside the cell was difficult to measure because multiple internal reflections from the polished stainless steel cell plates are possible. To estimate the laser power entering the cell, the cell mounting flange (including the ZnSe window, see Figure 2.9), support rod, and cell were removed from the vacuum chamber. The transmitter plate opposite the one through which the laser beam enters the cell was removed, and the beam was reflected from the gold mirrors, passed through the ZnSe window, reflected from the cell beam reflector (see Figure 2.8) and passed through the transmitter plate mesh while outside of the vacuum system. The laser power exiting the (open) analyzer cell under these conditions, identical to those used in actual experimentation, was 20 watts (approximately 2.5 less than the direct output of the laser). Assuming one internal reflection from the transmitter plate which had been removed for the above

measurement, and a 1-cm^2 cross-sectional area for the laser beam, an estimate of the actual irradiance to which the ions were subjected is 40 W cm^{-2}. For favorable cases, 100% dissociation was observed, indicating complete overlap of the laser beam and the trapped ion cloud.

A typical IRMPD experiment consisted of ion formation by electron impact (50 eV for 5 ms) followed by a reaction delay (0-1000 ms) to build up a significant concentration of protonated molecules via fragment-ion/molecule reactions. The reaction delay was not necessary when molecular ion dissociation was being investigated. The ion of interest was next isolated by ejection of all other ions, followed by gated laser irradiation of 200-2000 ms. Immediately after laser irradiation the ions were detected.

Collision-induced dissociation experiments were done similarly to those involving IRMPD except that an oscillating voltage, with a frequency equal to the cyclotron frequency of the ion to be accelerated, applied to opposing cell plates (typically for 100 microseconds) was used instead of laser irradiation to excite the ion to higher translational energies and a collision time of typically 10 ms was then allowed for dissociation. Sample pressure was maintained at ca. 3×10^{-8} torr, as measured on an ionization gauge. Argon or xenon was added as collision gas until the total pressure was in the $5\text{-}10 \times 10^{-7}$ torr range. The maximum kinetic energy to which ions can be accelerated in FTICR/CID experiments before they strike the walls of the analyzer cell is given (Cody and Freiser, 1982) by KE_{max} =

$e^2r^2B^2/(2m)$, where e is the charge of an electron, r is the cyclotron radius, B is the magnetic field, and m is the mass of the ion. In the experiments reported here, B = 3 tesla, r = 1.27 cm, and thus KE_{max} = 486 eV for protonated tripropylamine (m/z 144). To maximize the intensities of observed fragment ions, most CID experiments were done by exciting parent ions to kinetic energies very near the maximum allowable (400-800 eV depending on ion mass).

All chemicals were obtained commercially and sample purity was determined by electron impact mass spectrometry. No further sample purification was necessary except for several freeze-pump-thaw cycles to remove noncondensible gases.

Results and Discussion

Both the IRMPD and CID of molecular ions, protonated molecules and selected fragment ions of tri-n-propyl-, triethyl-, di-n-propyl-, di-isopropyl-, and diethyl-amine were studied. Results are listed in Table 5.1. For molecular ions, C-C bond cleavage and production of an immonium ion were observed for both means of dissociation. Protonated molecules, however, showed somewhat different behavior. Their dissociation when induced by laser irradiation generally involved C-N bond cleavage with some type of rearrangement, while CID proceeded via C-C bond cleavage and production of an immonium ion, or C-N bond cleavage and formation of an alkyl ion. Daughter ions produced by either IRMPD or CID fragmented further, typically by a mechanism similar to that which led to their

Table 5.1
Results for IRMPD and CID of selected alkylamines[a]

Amine Type of Ion (Mode of Formation)	Ion	IRMPD fragments (m/z)	CID fragments (m/z)
Tripropylamine			
M^+ (EI)	$(C_3H_7)_3N^+$ (m/z 143)	114	114,86,43
F^+ (IRMPD/CID)	$(C_3H_7)_2NCH_2^+$ (m/z 114)	86	86,43
F^+ (IRMPD/CID)	$C_3H_7(CH_3)NCH_2^+$ (m/z 86)	58	58,44,43
$(M + 1)^+$ (IMR)	$(C_3H_7)_3NH^+$ (m/z 144)	102	114,43
F^+ (IRMPD)	$(C_3H_7)_2NH_2^+$ (m/z 102)	60	60,43
Triethylamine			
M^+ (EI)	$(C_2H_5)_3N^+$ (m/z 101)	86	86
$(M + 1)^+$ (IMR)	$(C_2H_5)_3NH^+$ (m/z 102)	n.s.f.	74,58,29
Di-n-propylamine			
M^+ (EI)	$(C_3H_7)_2NH^+$ (m/z 101)	58	72,58,30,29
$(M + 1)^+$ (IMR)	$(C_3H_7)_2NH_2^+$ (m/z 102)	60	60,43,41,30,27
Di-isopropylamine			
M^+ (EI)	$[(CH_3)_2CH]_2NH^+$ (m/z 101)	86	86,44,43,27
$(M + 1)^+$ (IMR)	$[(CH_3)_2CH]_2NH_2^+$ (m/z 102)	n.s.f.	86,60,44,43
Diethylamine			
M^+ (EI)	$(C_2H_5)_2NH^+$ (m/z 72)	58	58,30,29
$(M + 1)^+$ (IMR)	$(C_2H_5)_2NH_2^+$ (m/z 74)	n.s.f.	58,30,29

[a]The following notation is used in Table 1: M^+ = molecular ion; $(M + 1)^+$ = protonated molecule; F^+ = fragment ion; (EI) refers to ions formed by electron impact; (IRMPD/CID) refers to ions formed by either IRMPD or CID; (IRMPD) refers to ions formed solely by IRMPD; (IMR) refers to ions formed by ion/molecule reactions; n.s.f. = no significant fragmentation was observed (fragment peak had S/N < 2). The CID fragment ion of highest intensity is underlined. High-resolution experiments showed that m/z 44 fragment ions produced by CID were $C_2H_6N^+$, m/z 43 ions were $C_3H_7^+$, m/z 30 CH_4N^+, m/z 29 $C_2H_5^+$, and m/z 27 $C_2H_3^+$.

formation. Detailed discussion of all dissociations is given below. Reactions observed only in IRMPD are labeled with a "P" (e.g., P1); reactions observed in CID are labeled with a "C" (e.g., C2); and reactions observed in both processes with "P/C" (e.g., P/C3).

Molecular ions

Both IRMPD and CID were observed for the molecular ions produced by electron impact on tri-n-propyl-, triethyl-, di-n-propyl-, di-isopropyl-, and diethyl-amine. In every case, IRMPD produced only one fragment which, except for di-n-propylamine, was also the most intense ion observed following CID. For most cases, production of the primary fragment ion could be explained by C-C bond cleavage, with formation of a stable immonium ion. Further dissociation of major fragments, usually producing yet another immonium ion, was generally observed. However, a different mechanism must be used to explain secondary fragmentations than that which holds for production of the original immonium ion. For the fragment ions, dissociation is postulated to occur via a mechanism involving hydrogen transfer and C-N bond cleavage.

The molecular ion of tripropylamine exhibits C_a-C_b bond cleavage to produce a m/z 114 ion (presumably of an immonium structure) during both IRMPD and CID:

$$(C_3H_7)_3N^+ \text{ --> } (C_3H_7)_2N{=}CH_2^+ + C_2H_5 \qquad \text{(P/C1)}$$

m/z 143 m/z 114

The same subsequent fragmentation of this immonium ion is produced by both CID and IRMPD, but dissociation in this

case occurs via a mechanism different from that which holds for the molecular ion. The m/z 114 ion dissociates to produce a m/z 86 ion, which in turn dissociates further to produce a m/z 56 ion:

$(C_3H_7)_2NCH_2^+ \rightarrow (C_3H_7)(CH_3)N{=}CH_2^+ + C_2H_4$ (P/C2)

m/z 114 m/z 86

$(C_3H_7)(CH_3)NCH_2^+ \rightarrow (CH_3)_2N{=}CH_2^+ + C_2H_4$ (P/C3)

m/z 86 m/z 58

Reactions P/C2 and P/C3 are both postulated to involve g-hydrogen transfer (see Figure 5.1) followed by ethylene expulsion via a McLafferty-type rearrangement (McLafferty, 1959; Boer et al., 1968; Smith and McLafferty, 1971). Similar rearrangements and fragmentations observed in slow metastable decompositions of immonium ions have been discussed by Bowen et al., 1980 and Bowen, 1982. Some additional fragments, listed in Table 5.1, were also produced by CID of the m/z 86 ion.

Molecular ions of triethyl-, diethyl-, and di-isopropyl-amine fragment by IRMPD and CID through a mechanism similar to that observed for tri-n-propylamine: C-C bond cleavage with formation of alkyl radicals and immonium ions:

$(C_2H_5)_3N^+ \rightarrow (C_2H_5)_2N{=}CH_2^+ + CH_3$ (P/C4)

m/z 101 m/z 86

$(C_2H_5)_2NH^+ \rightarrow (C_2H_5)HN{=}CH_2^+ + CH_3$ (P/C5)

m/z 73 m/z 58

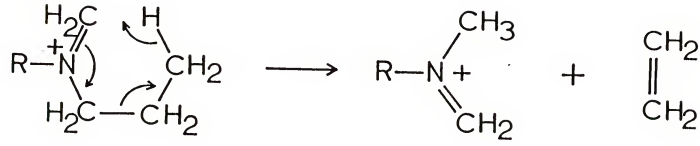

Figure 5.1. Loss of C_2H_4 postulated to occur via a McLafferty-type rearrangement.

$[(CH_3)CH]_2NH^+$ --> $[(CH_3)_2CHN{=}CHCH_3]^+ + CH_3$ (P/C6)

m/z 101 m/z 86

No further photodissociation of the m/z 86 immonium ion produced in reaction P/C4 was observed, consistent with the g-hydrogen transfer mechanism depicted in I. The activation energy barrier for direct C-N bond cleavage apparently is too high to be overcome during the IRMPD process.

Photodissociation of the triethylamine ion using a pulsed CO_2 laser has been reported by Haas and Lifshitz, 1980. Fragmentation as shown in reaction P/C4 was seen. Subsequent dissociation of the m/z 86 photofragment ion to form a m/z 58 ion, which fragmented further to produce m/z 30 and m/z 28 ions was seen by those workers. Similar photofragment ion dissociation was not observed in this work, probably because the relatively low irradiance of the CW CO_2 laser was not sufficient to excite these ions over apparently high barriers to dissociation.

Dissociation of the molecular ion of di-n-propylamine cannot be explained by a mechanism similar to that used for the other molecular ions studied. An ion with m/z 58 was produced by both IRMPD and CID:

$(C_3H_7)_2NH^+$ --> $C_3H_8N^+ + C_3H_7$ (P/C7)

m/z 101 m/z 58

The m/z 58 ion was the only fragment observed following IRMPD, but it was seen as a minor product following CID, while an m/z 72 ion $[(C_3H_7)HN{=}CH_2^+]$ was the most intense fragment, consistent with CID results for the other

molecular ions (C-C bond cleavage and immonium ion formation). No detailed explanation for the different IRMPD behavior of the di-n-propylamine molecular ion can be given at this time.

Protonated molecules

Numerous fragment ions were formed during electron impact ionization of the alkylamines studied in this work. Proton-transfer reactions of these fragments with alkylamine neutrals produced protonated molecules. Infrared laser irradiation of these ions resulted in C-N bond cleavage with hydrogen shift and loss of an alkyl group, producing an ammonium ion. In marked contrast, the major ion observed following CID was either an immonium ion resulting from C-C bond cleavage and loss of an alkyl radical, or an alkyl ion produced by C-N bond cleavage. This behavior was observed in both tri-n-propylamine and di-n-propylamine.

Tri-n-propylamine is protonated by ion/molecule reactions of the electron impact fragments $C_7H_{16}N^+$ and $C_5H_{12}N^+$:

$$\underset{\text{m/z 114}}{C_7H_{16}N^+} + (C_3H_7)_3N \rightarrow \underset{\text{m/z 144}}{(C_3H_7)_3NH^+} + C_7H_{15}N \qquad (1)$$

$$\underset{\text{m/z 86}}{C_5H_{12}N^+} + (C_3H_7)_3N \rightarrow \underset{\text{m/z 144}}{(C_3H_7)_3NH^+} + C_5H_{11}N \qquad (2)$$

When subjected to maximum laser irradiance (ca. 40 W cm^{-2}) the protonated molecular ion fragments to produce a m/z 102 ion,

$(C_3H_7)_3NH^+$ --> $(C_3H_7)_2NH_2^+ + C_3H_6$ (P1)

m/z 144 m/z 102

which photodissociates to produce a m/z 60 ion.

$(C_3H_7)_2NH_2^+$ --> $(C_3H_7)NH_3^+ + C_3H_6$ (P2)

m/z 102 m/z 60

This process is assumed to occur analogously to the reaction P1. A m/z 102 ion was also observed in the CID spectrum as a very minor peak. Experiments at lower collision energies with a triple quadrupole mass spectrometer (Johnson and Yost, 1985) confirmed this result.

Reaction P1 involves cleavage of a C-N bond and transfer of a hydrogen to the nitrogen atom. Considerable evidence has been amassed by earlier workers (vide infra) that this dissociation occurs via a loose complex. Stretching of the C-N bond (see Figure 5.2) gives rise to a complex (b) in which an incipient carbonium ion is coordinated to an amine. Slight rearrangement in (b) leads to (c), where an amine and olefin are bound to a common proton. Dissociation of (c) then occurs, and the proton remains with the neutral of highest proton affinity, in this case the amine.

This type of mechanism is discussed extensively by Moylan and Brauman, 1982, in explaining pulsed CO_2 laser IRMPD of protonated ethylisopropylamine, and was also frequently invoked by Bowen et al., 1982, and Bowen, 1980, to explain metastable decomposition of immonium ions.

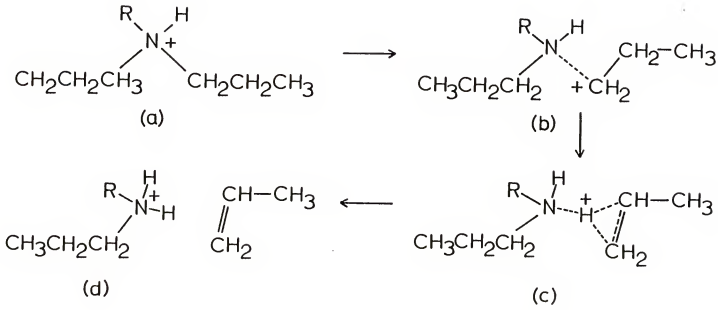

Figure 5.2. Loss of alkyl group proceeds through a proton bridged complex. Proton remains with amine as complex dissociates.

Alternatively, a mechanism which involves C-N bond cleavage and transfer of a g-hydrogen could explain the dissociation observed for protonated tri-n-propylamine as shown in Figure 5.3. Further support for this mechanism is provided by experimental results for IRMPD of protonante triethylamine and di-isopropylamine. For these ions, which have no available g-hydrogens, no significant dissociation was observed upon irradiation. However, dissociation of these ions via the proton-bridged loose complex mechanism shown in Figure 5.2 should be almost as facile as dissociation of protonated tri-n-propylamine.

The CID of protonated tri-n-propylamine gave rise to different products than IRMPD.

$$(C_3H_7)_3NH^+ \text{ (m/z 144)} \longrightarrow C_3H_7^+ \text{ (m/z 43)} + (C_3H_7)_2NH \qquad \text{(C1)}$$

$$(C_3H_7)_3NH^+ \text{ (m/z 144)} \longrightarrow (C_3H_7)_2NCH_2^+ \text{ (m/z 114)} + C_2H_6 \qquad \text{(C2)}$$

Reaction C1 involves a simple C-N bond cleavage and requires an overall enthalpy of 368 kJ mol^{-1}. The second reaction, however, is more complicated. A hydrogen migration from N to a b-C is necessary to form the m/z 114 immonium ion and an ethane molecule. A possible mechanism is given in Figure 5.4.

Di-n-propylamine is protonated by ion/molecule reactions involving the fragment ions $CH_2NH_2^+$, $C_2H_6N^+$, and $C_3H_7NHCH_2^+$, formed by electron impact:

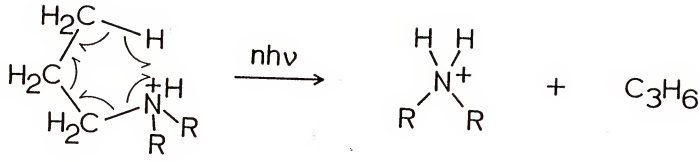

Figure 5.3. Alternative mechanism for loss of alkyl group proceeds via transfer of a gamma-hydrogen.

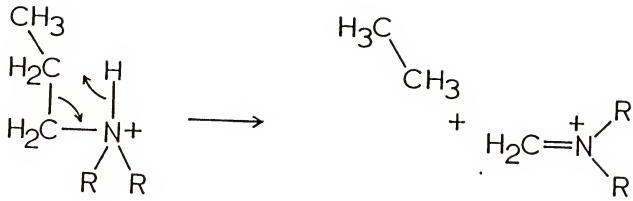

Figure 5.4. Possible mechanism to account for loss of ethane.

$CH_2NH_2^+ + (C_3H_7)_2NH \rightarrow (C_3H_7)_2NH_2^+ + CH_3N$ (3)
m/z 30 m/z 102

$C_2H_6N^+ + (C_3H_7)_2NH \rightarrow (C_3H_7)_2 + C_2H_5N$ (4)
m/z 44 m/z 102

$(C_3H_7)NHCH_2^+ + (C_3H_7)_2NH \rightarrow (C_3H_7)_2NH_2^+ + C_3H_7NCH_2$ (5)
m/z 72 m/z 102

Protonated di-n-propylamine photodissociates by reaction P2 producing a m/z 60 $(C_3H_7)NH_3^+$ ion. Collision-induced dissociation of protonated di-n-propylamine produces $C_3H_7^+$ (m/z 43) and $C_3H_7NH_3^+$ (m/z 60). Formation of the m/z 60 $C_3H_7NH_3^+$ ion is postulated as taking place via a mechanism identical to the IRMPD of this ion shown in reaction P2.

No photodissociation of protonated di-isopropylamine or diethylamine was observed. Because these ions contain no g-hydrogens, the observed results are more consistent with the mechanism shown in Figure 5.3 than that shown in Figure 5.2. More definitive evidence as to the importance of g-hydrogen transfers could be provided by study of alkylamines labeled with deuterium at that position. Limited deuterium-labeling experiments were done by transferring a deuteron from D_3O^+ to the amines. The deuterium atom was retained on the amine after alkene loss, indicating no hydrogen transfer between the nitrogen and carbon atoms in the protonated amines. As would be expected, this type of experiment gives no information as to whether Figure 5.2 of Figure 5.3 is operative. The deuterium atom was lost in reaction C2, supporting the validity of Figure 5.4. Experiments

involving synthesis and study of alkylamines with deuterium on the g-carbon are needed in order to elucidate the proposed mechanisms.

Infrared multiphoton dissociation was observed to proceed only via the fragmentation pathway of lowest activation energy. Collisional and radiative energy loss processes compete with absorption of infrared photons during the several hundred milliseconds of irradiation time usually required when a gated CW CO_2 laser is used in this process. This limits the amount of internal energy which can be deposited into an ion to ca. 160-250 kJ mol^{-1}. If the barriers to fragmentation for all pathways are higher than this range, no dissociation is observed. Such appears to be the case for protonated di- and tri-ethylamine and di-isopropylamine. For protonated di- and tri-n-propylamine, C-N bond cleavage with accompanying hydrogen transfer to the nitrogen atom, whether it takes place via the scheme shown in Figure 5.2 or 5.3, has sufficiently low activation energy that it can be observed by IRMPD. Results on collision-induced dissociation for these two ions show formation of alkyl ions via direct C-N bond cleavage as the major fragmentation process. These fragmentations have a higher energy, but lower entropy, of activation and should be favored in CID, which can impart much higher internal energies to ions than IRMPD. [Fragmentation ratios for CID experiments can vary dramatically with collision energy. The results reported here correspond to energies in the range 400-800 eV (vide ante). In one series of experiments

involving protonated tri-n-propylamine ion, kinetic energies were successively lowered to the 5-20 eV range. At these ion collision energies, the m/z 102 ion, observed exclusively following IRMPD, was the major CID fragment, although quite low in intensity when compared to its formation by IRMPD or to the m/z 43 ion formed at higher collision energies.] The fact that the only fragment ion produced by infrared irradiation is either not formed (in protonated tri-n-propylamine dissociation) or seen only as a minor fragment (in protonated di-n-propylamine dissociation) during the CID process lends further support to the fragmentation mechanism shown in Figure 5.3, which involves a tight transition state. In cases where CID results only were observed (protonated di- and tri-ethylamine and di-isopropylamine) the major fragment ion was often produced by a high-energy process (e.g., 368 kJ mol^{-1} (Aue and Bowers, 1979; Franklin et al., 1969) for reaction C1), attesting to the higher range of internal energies deposited in the ions during the CID process.

Earlier chapters have demonstrated the potential of IRMPD for isomeric differentiation. It is interesting to note that both parent and protonated di-n-propylamine and di-isopropylamine ions exhibit substantially different photodissociation behavior (Table 5.1). As can be seen in Table 5.1, CID can be used for isomeric differentiation as well.

In summary, significant differences between IRMPD and CID were seen for protonated amines, but unprotonated

molecular ions behaved similarly under both dissociation processes. In contrast to the work on oxygenated compounds where C-O bonds and not C-C bonds were broken, some of the amines in this study preferentially underwent C-C and not C-N bond cleavage.

CHAPTER 6
COLLISIONAL QUENCHING OF VIBRATIONALLY EXCITED IONS

Gaseous ions formed from interactions of molecules with intense light or high-energy electrons possess a distribution of internal energies. This internal energy can be distributed among electronic, vibrational, and rotational states. This distribution influences the ions' response to their environment; that is, whether they spontaneously decompose to form fragment ions, react through certain reaction pathways, or rearrange to different structures. In this chapter the role ion/molecule collisions play in altering the internal energy distributions of gaseous ions will be explored. The collisional deactivation of vibrationally excited protonated 1,2-dimethoxyethane, ethyl acetate, and bis(2-methoxyethyl)ether (diglyme) are explored using the corresponding neutral molecule, argon, helium, and nitrogen as collisional quenching gases. A model which takes into account the infrared pumping, radiative, and collisional quenching of the ions under study is discussed.

Much work on collisional deactivation has been done with neutral/neutral systems, but relatively few studies of ion/neutral systems have been performed (vide infra). The ion/neutral experiments generally fall into two categories, those involving diatomic ions and those involving polyatomic ions. The diatomic studies involve cases where state

specific information is available, and detailed conclusions about energy transfer can be drawn. Many vibrational quenching studies involving diatomic ions have been carried out using both flow-drift tubes (DRIFT) and selected ion flow tubes (SIFT) (McFarland et al., 1973; Smith and Adams, 1979). In contrast, for polyatomic ions, usually no state-specific information is available and only gross changes in energy levels such as changes in the amount of fragmentation or dissociation are observed. Much of the work on polyatomic ions has been performed using ion cyclotron resonance (ICR) to trap the ions and various laser techniques to probe the amount of vibrational excitation (Rosenfeld et al., 1982; Dunbar, 1984; Kemper and Bowers, 1984). The laser techniques most often employed are 2-photon photodissociation (2PPD) and infrared multiphoton photodissociation (IRMPD) (vide infra).

The work presented here is concerned with collisional deactivation of polyatomic ions when they are pumped to highly excited vibrational levels by infrared laser radiation. The ions are irradiated until there is a high probability that their internal energy exceeds the activation energy barrier beyond which fragmentation can occur. An increase in abundance of the neutral background molecules results in collisional deactivation of the excited ions which drastically alters the apparent photodissociation cross-section. Such effects must be taken into account for experiments which measure absolute and relative cross-sections because the population levels of highly excited

ions are especially sensitive to vibrational quenching by collisional deactivation.

Differences in the photodissociation yields are most often used to quantitate collisional quenching efficiency in larger polyatomic experiments. ICR experiments using both 2PPD (Kim and Dunbar, 1979; Dunbar and Ferrara, 1985) and IRMPD (Woodin et al, 1979; Bomse et al., 1979; Jasinski et al., 1982; Rosenfeld et al., 1982) have probed the quenching efficiency of various neutrals with polyatomic ions. In 2PPD a visible laser pulse excites the ion to high internal energy below the dissociation barrier. At some later time a second visible laser pulse pumps the ions over the dissociation barrier. A variable time delay is introduced between the two laser pulses. If the ion is allowed to deactivate collisionally before the second laser pulse, a decrease in the photodissociation yield is observed.

Infrared multiphoton dissociation using both pulsed and continuous wave infrared lasers involves the sequential absorption of many infrared photons (Thorne and Beauchamp, 1984) until the lowest dissociation barrier is overcome and the ion fragments. Experiments that utilize pulsed laser IRMPD to probe collisional quenching (Jasinski et al., 1982; Rosenfeld et al, 1982) usually involve the formation of hot ions by exoergic ion/molecule reactions. A portion of this excess internal energy is available as vibrational excitation, and the ions are predisposed to photodissociate when irradiated by a pulsed infrared laser. Should these "hot" ions be relaxed by collisions with neutrals before

irradiation, then the observed photodissociation yield decreases. Introduction of various collision gases and observation of changes in total photodissociation yield reflect the collisional deactivation efficiency.

Alternatively, as in the work presented here, a relatively low-power infrared laser can be used to bathe ions with infrared photons, and at sufficiently low photon fluxes and relatively high neutral pressures, collisional deactivation successfully competes with photodissociation. The change in the amount of photodissociation, measured as the neutral pressure is increased, monitors the collisional deactivation efficiency of the neutral buffer gas.

Experimental

Ions were formed and trapped in a Nicolet FT/MS-1000 Fourier transform ion cyclotron resonance mass spectrometer (FTICR) by conventional electron impact (EI) ionization. The electrons were accelerated to either 20 eV (20 ms beam duration) or 50 eV (5 ms beam duration) for these experiments. After ionization a suitable delay (1 s typically) was introduced so that protonation reactions between the EI fragments and the neutral background molecules produced significant amounts of the protonated molecule in the analyzer cell. Following this reaction period all ions other than the protonated molecule were ejected.

After removing all other ions except the ion of interest, another delay was introduced during which light

from an infrared laser irradiated the ions. The irradiation period was controlled by means of a solenoid driven shutter which could be gated open and closed by a trigger pulse from the FTICR. Light from the laser was reflected to a power meter when the shutter was in the closed position. For all experiments reported below the laser was operated at a wavelength of 10.61 microns. The output power was adjusted to 1.0 watts as measured from the beam reflected from the partially reflective shutter. Positions of all other laser optics were identical to those described in the instrumentation chapter (see Chapter 2, p 24).

For these experiments the sample and buffer gas pressure ranged from 10^{-8} to 10^{-6} torr as measured by an ionization gauge. Base pressure for the sample compound was typically 1×10^{-7} torr. Buffer gas pressure could be increased until the total pressure reached 9×10^{-6} torr. The pressures for argon, helium, and nitrogen were corrected by dividing partial pressure by the ionization gauge sensitivity factor as supplied by the manufacturer. The sensitivity factor for 1,2-dimethoxyethane and diglyme was not available but were estimated to be similar to those for ethyl acetate and diethyl ether.

All samples were obtained from commercial sources and sample purity was determined by electron impact mass spectrometry. Residual noncondensible gases were removed by several liquid nitrogen freeze-pump-thaw cycles. No further sample purification was necessary.

Results and Discussion

The collisional quenching rates of diatomic ions with various neutrals have been reported and vary from the Langevin rate constant to less than 10^{-12} cm^3/s (Ferguson, 1986). These values for rate constants reflect energy transfers needed for deactivation ranging from one collision to more than 1000 collisions. For all diatomic ions no significant vibrational deactivation was observed for collisions with He and Ne, which have vibrational quenching rate constants of less than 10^{-12} cm^3/s. The collisional deactivation efficiency increases with mass and polarizability of the collision partner. The collisional quenching of an ion with its parent neutral was usually extremely fast at near-Langevin rates. These fast ion/neutral reactions are thought to be symmetric charge transfer reactions.

Quenching with argon, helium and nitrogen

It was observed that the amount of photodissociation of the protonated molecules of 1,2-dimethoxyethane, ethyl acetate, and diglyme decreased when argon, helium, or nitrogen was added (see Figure 6.1). The collisional quenching efficiency followed similar trends observed for these buffer gases on diatomic ions (Dobler et al, 1983; Bohringer et al, 1983; Ibuki and Sugita, 1983; Ferguson, 1984). The observed trend was that helium was a less efficient quenching gas than argon, and argon was less efficient quencher that nitrogen. This trend is well

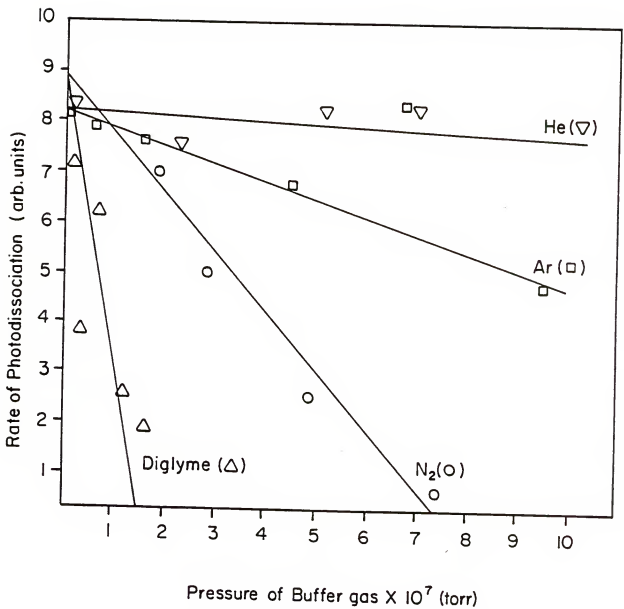

Figure 6.1. Rate of photodissociation for protonated diglyme decreases as a function of buffer gas.

illustrated in Figure 6.2. For argon and helium the loss of vibrational energy from the excited ions can only occur by a vibrational to translational energy transfer. The possibility of efficient resonance vibrational to vibrational energy transfer from the excited ion to nitrogen is conceptually possible but not realistically probable since the vibrational frequencies differ drastically. The greater nitrogen quenching efficiency may be attributed to this molecule's higher polarizability compared to argon. This results in nitrogen having a higher Langevin collision rate. The Langevin collision rates for helium, argon, and nitrogen with a protonated diglyme molecule are 1.8×10^{-9}, 1.9×10^{-9}, and 2.2×10^{-9} cc/s, respectively.

For simple diatomic ions, collisional quenching has been successfully described by formation of an intermediate complex in which vibrational predissociation competes with unimolecular dissociation back to reactants (Ferguson, 1984). Both the decrease in quenching efficiency with increased kinetic energy and the increase with larger more polarizable buffer molecules are consistent with complex formation. Once the complex is formed, it can unimolecularly decay back to reactants or vibrationally predissociate to yield products. The model is represented below:

$$AB^+(v) + X \longrightarrow [AB^+(v)\text{-}X]^{\ddagger} \longrightarrow AB^+(v'<v) + X$$

where k_c, k_u, and k_{vp} are the rate coefficients for complex formation, unimolecular decomposition back to reactants, and

INFRARED PUMPING

$$A_0 \xrightarrow[k_{p1}]{h\nu} A_1 \xrightarrow[k_{p2}]{h\nu} A_2 \cdots \xrightarrow[k_{pn}]{h\nu} A_n$$

SPONTANEOUS INFRARED EMISSION

$$A_n \xrightarrow[k_r]{h\nu} A_{n-1}$$

COLLISIONAL QUENCHING

$$A_n + M \xrightarrow[k_c]{} A_{n/2} + M$$

Figure 6.2. Main features for the kinetic simulation model.

vibrational predissociation. The overall quenching rate, k_q is given by,

$$k_q = k_c * (k_{vp} / (k_u + k_{vp}))$$

and can be thought of as the product of the rate of complex formation times the fraction of the complexes that vibrationally predissociate. This model has also been successfully employed to explain dissociation of bound neutral van der Waals molecules (Levy, 1981). The experimental results are consistent with predissociation occurring on approximately a 10^{-9} s time scale (Ferguson, 1984), and for cases where k_{vp} has been determined the model seems insensitive to the nature of the complex. Generally, one quantum of energy is transferred to the complex bond (Bohringer et al., 1983) resulting in dissociation. This process can be thought of as a vibration to vibration transition leading to an overall vibration to translation transition as the complex dissociates. Vibration to rotation transitions are also possible, but such effects are expected to be small (Dunbar and Ferrara, 1985). Resonance vibration to vibration transitions (Ferguson et al.,1984) have not been observed and are not thought to be important for collisions of small diatomic ions with small buffer gases, but may be significant for larger ions.

Quenching with the parent neutral

For the protonated molecules of 1,2-dimethoxyethane, ethyl acetate, and diglyme, a drastic decrease in the amount of photodissociation was observed when the pressure of the

neutral molecule was increased (see Figure 6.1). In all cases reported here the quenching rate was found to vary nearly linearly with pressure and time. These observations of the quenching of polyatomic ions by their corresponding parent neutrals have also confirmed the fact that large polyatomic buffer gasses have a larger quenching efficiency than the smaller atomic and diatomic gases. Dunbar and Ferrara, 1985, have shown that deuterated buffer gases show a slight increase in the quenching efficiency consistent with the observed increase in mass seen in diatomic cases.

The model of deactivation by vibrational predissociation makes no assumptions about the ion's role in the complex formation. Polyatomic ions are equally likely to form intermediate complexes, and therefore the vibrational predissociation model should apply equally well. However, the amount of vibrational quenching as measured by the drastic decrease in the amount of photodissociation does not support the assumption that only one quantum of energy is transferred per collision, and this assumption may not be valid for the complexes of large polyatomic ions with large polyatomic neutrals. Expanding this model to include the transfer of several vibrational quanta, such as allowing efficient vibrational to vibrational energy transfer to occur, provides a reasonable quenching mechanism for polyatomic ions.

In order to test various collisional quenching mechanisms, kinetics simulations of the photodissociation process were performed. To aid these studies the

photodissociation rate of diglyme was experimentally determined as a function of pressure. A realistic model which reproduces the experimental data is presented.

Kinetics Model

The three major processes that make up the photodissociation kinetics model are shown in Figure 6.2. These processes include vibrational state to state reactions for infrared pumping, spontaneous infrared emission, and collisional quenching. Each process consists of a number of individual steps corresponding to changes in discrete vibrational levels. The total number of steps was limited to 40 by the particular kinetics integration computer program used. The Gear integration (Gear, 1978) method was employed and from the 40 individual reaction steps a total of 40 simultaneous differential equations were solved to yield the kinetics data.

Infrared pumping was accomplished by allowing the absorption of one infrared photon to promote an ion from the n to the n+1 state. A total of 14 pump steps were allowed before dissociation occurred. At a laser wavelength of 10.61 microns this would correspond to a molecule absorbing 39 kcal/mol of energy. This amount of energy is clearly much less than that needed to cleave an ordinary C-O bond, but simple thermochemical calculations (Baykut et al., 1985) have shown that protonation greatly reduces the C-O bond strength. The actual number of photons necassary for dissociation may be greater than 14, but this number

represents the limit for this model. It was assumed that upon reaching the dissociation barrier (absorption of 14 photons) that fragmentation occurred immediately without further photon absorption. This assumption is similar to one made in another modeling study (Lev and Dunbar, 1983) which investigated the photodissociation yield enhancement of infrared irradiation on visible laser photodissociation.

Several pumping mechanisms were investigated. These included reaction steps where the rate of pumping increased with internal excitation, decreased with internal excitation, remained constant, and one mechanism where the first level involved a bottleneck followed by fast pumping. The mechanism where the rate of pumping up the discrete levels remained constant best fit the experimental data. A pseudo-first order rate constant consisting of the product of the absorption cross section and the photon flux of 70 s^{-1} was chosen because it gave the best fit to the experimental data. The absorption cross section can be obtained by dividing this rate by the estimated photon flux. The estimated photon flux is 3.8 X 10^{20} photons/(cm^2 s) and dividing this into the pumping rate yields a value of 1.8 X 10^{-19} cm^2 for the absorption cross section. This pumping mechanism is consistent with either the ion being in the vibrational quasicontinuum (Thorne and Beauchamp, 1984) or with previously proposed (see Chapter 1) pump-dump model (Tamir and Levine, 1977).

Rates for spontaneous emission of photons from various compounds have been reported which range from 1 to 100 s^{-1} (Dunbar, 1984). It has been observed that the rate of stimulated emission increases as a function of internal vibrational excitation (Dunbar, 1975). The rates for spontaneous infrared emission for toluene have been calculated to vary from 1 to 66 s^{-1} (Dunbar, 1975). Based on this information the rates for spontaneous emission were estimated to vary from 1 s^{-1} for the n=1 level to 92 s^{-1} for the n=13 level in increments of 7 s^{-1}.

The drastic decrease in the amount of photodissociation for the protonated molecules with increasing pressure of the corresponding neutral molecule is postulated to occur through formation of a ion/neutral intermediate complex. This complex is believed to be very short lived on the ICR time scale at lower pressures, but at higher pressures collisional stabilization of the complex can occur. At lower pressures the complex is postulated to have a long enough lifetime that complete energy randomization occurs between the excited ion and neutral before the complex dissociates. This is modeled by having an excited ion in the n level drop back to the n/2 level during the collisional encounter. The rates for these collisional quenching reactions were varied until agreement between the experimental and simulated data was obtained. It was assumed that the quenching efficiency was constant for all vibrational levels above the ground state.

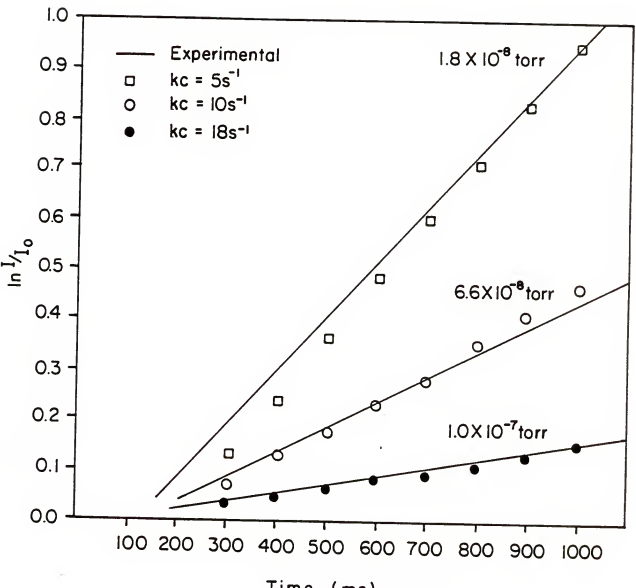

Figure 6.3. Comparison of experimental data (soild lines are least squares fit to the experimental data) and results obtained from the kinetic model (individually plotted points).

Shown in Figure 6.3 is a plot of relative cross section versus time for the experimental and calculated data at several diglyme pressures. For each set of pressure data the rate of collisional quenching was obtained by dividing the pseudo-unimolecular rate (5 s^{-1} for 1.8 X 10^{-8} torr; 10 s^{-1} for 6.6 X 10^{-8} for; and 18 s^{-1} for 1.0 X 10^{-7} torr) by the concentration of neutral molecules. An average value for the rate of collisional quenching of 8.6 X 10^{-9} cc/s was obtained from the simulated data. To serve as a check on the validity of the magnitude of this rate constant an experiment was performed to measure the rate of diglyme self-protonation reactions. Self-protonation and collisional quenching rate constants are expected to be similar since these two reactions both involve formation of a collisional complex. Upon formation of the collision complex complete energy randomization is expected and for both cases proton transfer occurs.

The rate of diglyme self-protonation was determined by isolating the naturally occurring ^{13}C isotope ion and allowing it to react with the background neutral molecules. The rate of production of the normal ^{12}C protonated molecule was measured. The rate was found to be 2.4 X 10^{-9} cc/s. Even though these rates differ by a factor of four they are in the same neighborhood and this seems to support the complex formation/ energy randomization mechanism.

Conclusion

The model of vibrational predissociation of an ion/molecule complex which has been used to describe vibrational deactivation of diatomic ions can be expanded when studying larger polyatomic ions, provided that more than one quantum can be transferred along the complex's bond before dissociation of the complex occurs. This model does allow for complete energy randomization. The rapid quenching rate suggests the possibility of efficient resonance vibrational to vibrational energy transfer occurring while the ion and parent neutral are in intimate contact.

The discrepancy between the calculated collisional quenching rate and the self-transfer could result from the possible erroneous assumption that the internal energy is completely randomized throughout the collision complex. Dunbar and Ferrara, 1985, have recently reported results which suggest that for iodobenzene complete energy randomization does not occur. The kinetics reaction scheme presented here does adequately model the observed experimental data. Another possibility is that this discrepancy could result from the fact that the kinetics model does not consider the possibility of proton transfer reactions.

This model is by no means the only model which could reproduce the experimental data given the large number of variables which can be manipulated to fit the data. However, it does represent a realistic approach to a very

complicated system and can serve as a guide until more detailed information and/or a more sophisticated models about the photodissociation process are available.

CHAPTER 7
LASER PHOTODISSOCIATION OF GASEOUS IONS FORMED BY LASER DESORPTION

Introduction

The technique of laser desorption (LD) has been widely used in mass spectrometry (Conzemius and Capellen, 1980; Hillenkamp, 1983) to desorb and ionize high molecular weight or other nonvolatile samples, most often using time of flight (Tabet and Cotter, 1983; Van Breemen et al., 1983) or Fourier transform ion cyclotron resonance (FTICR) (McCrery et al., 1982; Wilkins et al., 1985) mass spectrometers for mass analysis. A sample is inserted into the vacuum system of a mass spectrometer where it is desorbed and ionized by focused laser irradiation, most often with a power density of ca. 10^6 W/cm^2.

The primary advantage of laser desorption is that abundant molecular or pseudo-molecular ions are produced for many different classes of compounds. Positive pseudo-molecular ions are most often formed by attachment of a cation, typically a proton, potassium or sodium ion, to the parent molecule. Negative pseudo-molecular ions can also be formed by laser desorption, usually by loss of a proton. Often little fragmentation occurs and the strong molecular ion signal [M^+, $(M+H)^+$, $(M+Na)^+$, $(M+K)^+$, M^- or $(M-H)^-$] provides molecular weight information.

Although an abundant molecular ion peak is important in identifying the molecular weight of a compound, fragmentation is often desirable to characterize the molecular and/or ionic structure. Several techniques have been applied to produce fragmentation; most notable are collision-induced dissociation (Levsen and Schwartz, 1983) and photodissociation (Thorne and Beauchamp, 1984). Thus, it would be advantageous to combine one of these techniques with laser desorption to obtain both molecular weight and structural information. One possible drawback of collision-induced dissociation is the difficulty in dissociating larger ions (Amster et al., 1983; Sheil and Derrick, 1985; Bowers et al., 1986) because of the inability to impart sufficient internal energy to them in collisions with much lighter target gas molecules. Also, energy sufficient to dissociate a smaller ion could be "lost", that is, randomized along the many vibrational modes of a significantly larger ion resulting in a dissociation lifetime longer than the ion's transit time in a conventional mass spectrometer. However, irradiative pumping of moderately large molecular compounds by infrared lasers has been observed to bring about photofragmentation (vide infra). In this chapter the successful combination of the laser desorption (LD) and photodissociation (PD) techniques is reported.

Experimental

Experiments were carried out in a Nicolet FT/MS-1000 mass spectrometer. The important features of this technique have been described elsewhere (Comisarow, 1985). The standard laser desorption interface supplied by the manufacturer was used. As shown by the solid line in Figure 7.1, light from a Lumonics TE 860 grating-tuned pulsed CO_2 (infrared) laser (PIRL) entered the vacuum chamber through a zinc selenide window and was focused by a ZnSe lens of 1.25 cm diameter and 5 cm focal length onto a solids probe containing the analyte. An Apollo 570 continuous wave grating-tuned CO_2 (infrared) laser (CWIRL) was also employed for laser desorption by gating the beam on and off to obtain a 25 ms pulse. However, its output was of insufficient power density to generate ions reliably and so its usage was limited.

Both the PIRL and CWIRL were employed for the photodissociation of gaseous ions produced by laser desorption. The CWIRL has maximum output power of 50 watts at 10.61 microms and a beam diameter of 6 mm. The PIRL produces 2.6 Joules in a pulse of one microsecond duration at 10.61 microns and has a 2 X 3 centimeter rectangular beam shape. Earlier modification of the FTICR for photodissociation studies (Baykut et al., 1985) have been previously reported and are discussed below in the "one laser" experiment. In the "two laser" experiment the conventional solids probe was replaced by a NaCl window mounted on a hollow tube (SWT) which extended into the

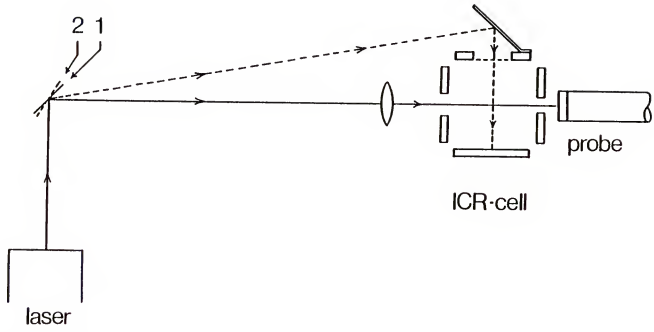

Figure 7.1. Configuration used for single laser experiments with a pulsed CO_2 laser. During the first laser pulse the beam is focused through the lens and forms ions by laser desorption. A rotatable mirror directs the second, unfocused laser pulse into the cell to fragment trapped ions by multiphoton dissociation.

vacuum chamber to within a few millimeters of the FTICR cell. The analyte was dissolved in either acetone or ethanol and deposited using a micropipette on the end of the tube opposite the window and nearest the cell. This assembly, shown in Figure 7.2, served as both sample support and as a second window for laser irradiation of the ions.

Samples were obtained from commercial sources where available or submitted from various research labs. Sample purity was confirmed by wide range mass spectra and the samples were used without purification.

Results and Discussion

Laser desorption with the (gated) continuous wave laser. Initial attempts to perform LD with the CWIRL were of limited success. Although, K^+ and $(M+K)^+$ from a sucrose sample were observed, low signal-to-noise (S/N) ratios and lack of reproducibility hindered these experiments. A 25 ms gated pulse from the CWIRL used for LD had a focused power density of ca. 2×10^3 W/cm^2. This is substantially below the currently accepted lower limit (Van Der Peyl et al., 1982) for reliable LD results. It was observed, however, that reasonably intense and reproducible ion signals could be obtained for preformed ions using the gated CWIRL. For example, both the organic cation and perchlorate anion of rhodamine-6G perchlorate were observed in the positive and negative LD mass spectra, respectively.

Laser desorption with the pulsed laser. The PIRL had sufficient power to produce abundant ions and substantial

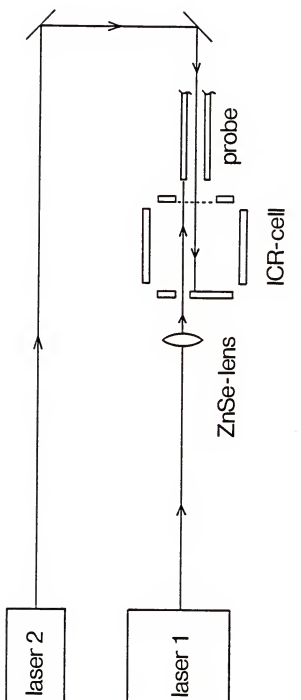

Figure 7.2. Configuration used for double laser experiment. A pulsed CO_2 laser (laser 1) is used to desorb and ionize the sample and a CW CO_2 laser (laser 2) is used to dissociate the trapped ions.

molecular ion intensity has been observed in approximately 90% of the samples analyzed to date. Excellent S/N and fair reproducibility were usually obtained.

Photodissociation of large ions. Isomeric differentiation studies by photodissociation (Baykut et al., 1985) and comparison of photodissociation with collision induced-dissociation in FTICR (Watson et al., 1985) have shown the usefulness of the former in obtaining structural information about relatively small gaseous ions. The work reported here resulted from the successful attempts to extend PD methods to much larger ions. These larger ions, with their many degrees of freedom and higher density of states, are expected to appear "black" in the infrared region; that is, their infrared absorption spectrum should be nearly continuous, leading to a high probability that they will absorb infrared laser photons. The question of whether internal excitation produced by infrared absorption would be relaxed by radiative or collisional processes faster than it might accumulate in certain modes leading to bond rupture was of great interest. Initially, three different larger molecular weight samples gently heated on a solids probe and ionized by electron impact were studied. The three ions discussed below underwent photodissociation after being subjected to gated output of 0.5 to 2 s duration from the CWIRL under conditions similar to those reported for smaller gaseous ions (Baykut et al., 1985). An ion of nominal m/z 442 was produced from cis-dichloro-trans-dihydroxobis-2-propanamine platinum (IV) (CHIP) by the

ion/molecule reaction (IMR) of the major electron impact (EI) fragment ion with the neutral molecule. As shown in Figure 7.3, this ion dissociated to produce two daughter photofragment ions, m/z 366 and m/z 311, by loss of various ligands.

$$m/z\ 442 + nhv \text{ ---> } m/z\ 366 \text{ and } m/z\ 311 \qquad (7.1)$$

Shown in Figure 7.4 is the photodissociation of protonated N,N'-bis(4,6-dimethylsalicylidene)-4-trifluoromethyl-o-phenylendiiminato cobalt (II) (CoSALOPH) which is also produced by the ion/molecule reactions of electron impact fragments with the neutral molecule. This ion dissociates by loss of a methyl group.

$$m/z\ 563 + nhv \text{ ----> } m/z\ 548 \qquad (7.2)$$

The ion produced by electron attachment to tris-n-nonylfluorotriazine dissociated in a 2-step consecutive pathway as shown in Figure 7.5.

$$m/z\ 1488 + nhv \text{ ---> } m/z\ 1069 + mhv$$
$$\text{---> } m/z\ 650 \qquad (7.3)$$

The above examples show that infrared multiphoton dissociation of large molecular ions can occur readily. This dissociation technique was next coupled with production of high molecular weight ions via laser desorption.

Use of a single laser for desorption/dissociation. Photodissociation of small gaseous ions by a PIRL has been reported (Jasinski et al., 1982), so an attempt was made both to form ions and to photodissociate them with sequential laser pulses from the same PIRL using the irradiation scheme shown in Figure 7.1. As shown in Figure

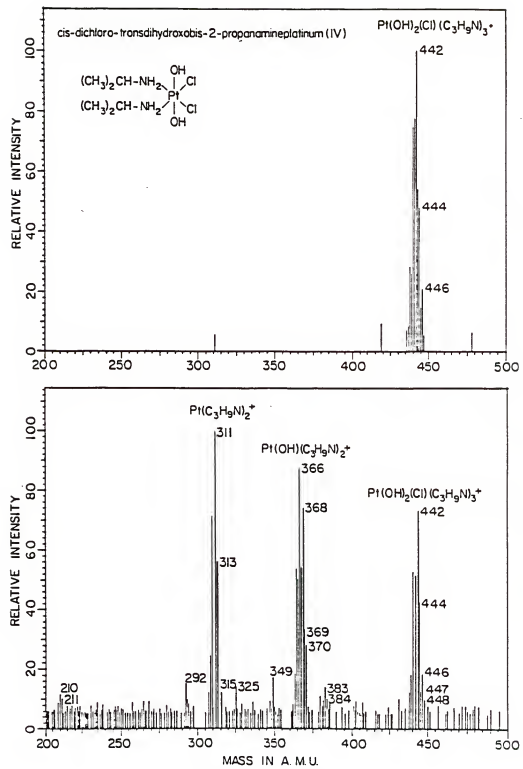

Figure 7.3. Top. Ion/molecule reaction product formed by reaction of cis-dichloro-trans-dihydroxo-bis-2-propanamine platinum (IV) with its electron impact fragments. Bottom. Fragmentation pattern produced upon irradiation with CW CO_2 laser, same experimental conditions and delay times as in the top spectrum.

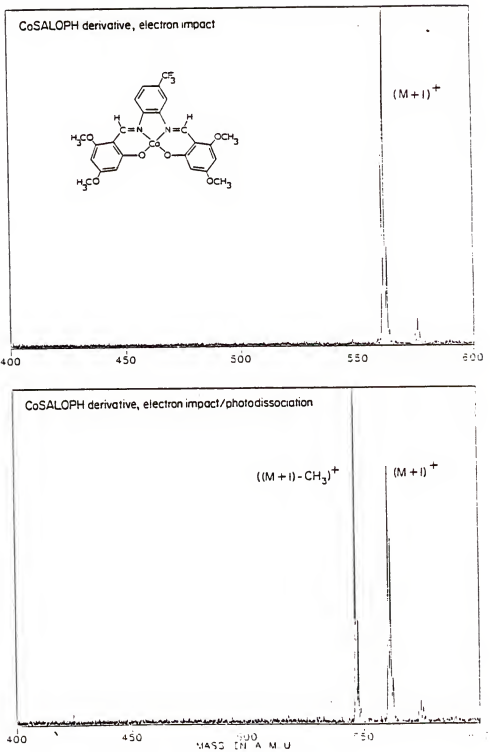

Figure 7.4. Top. Protonated N,N'-bis(4,7-dimethyl-salicylidene)-4-trifluoromethyl-o-phenyl-endiiminato cobalt (II) (CoSALOPH) formed by reaction of the neutral molecule with fragment ions produced by electron impact. Bottom. Fragmentation obtained upon irradiation with the CW CO_2 laser, same experimental conditions and delay times as in the top spectrum.

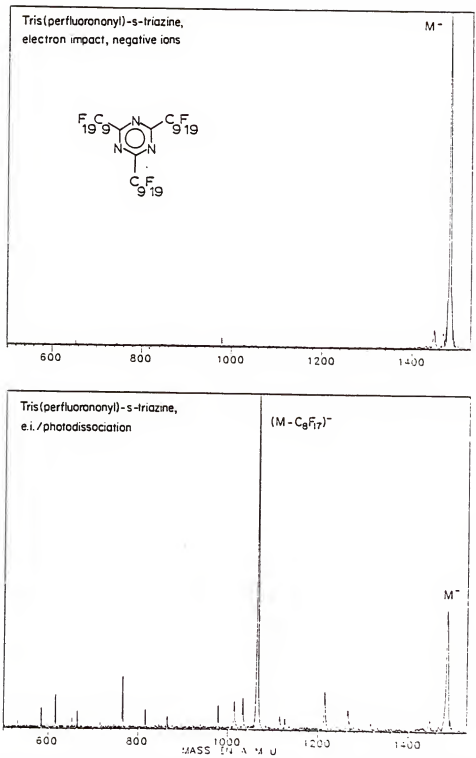

Figure 7.5. Top. Negative molecular ion of tris-n-nonyl fluorotriazine formed by electron capture. Bottom. Fragmentation obtained upon irradiation with CW CO_2 laser, same experimental conditions and delay times as in the top spectrum.

7.1 the ions were desorbed by a single laser pulse using a focusing lens, and then a mirror outside the vacuum chamber was rotated so that a second unfocused laser pulse entered the analyzer cell and irradiated the ions. The external mirror was then returned to its original position for the next experiment. Unfortunately, a very large K^+ signal was observed for both the focused and unfocused pulses. The potassium source is thought to be the insulating ceramic used in the FTICR cell. This large K^+ signal could be reduced somewhat by adjusting various delay times and ejecting this ion during the laser beam duration and for 50 ms following the end of the laser pulse. Time resolved LD mass spectrometry (Van Breemen et al., 1983) has shown that significant amounts of K^+ are formed for up to 30 ms following the laser desorption pulse. Under these ejection conditions photodissociation of the cation produced by laser desorption of the tertbutylpyridinium (TBP) cation (from the perchlorate salt) was observed. As shown in Figure 7.6 the TBP cation, m/z 136, dissociates under laser irradiation with loss of C_4H_8 to produce an ion of m/z 80, which is most likely protonated pyridine.

$$m/z\ 136 + nhv \text{ ---> } m/z\ 80 \qquad (7.4)$$

Use of two lasers for desorption/dissociation. Difficulty in eliminating the potassium ion formed during the second laser pulse and slight misalignment of the laser beam when moving the external mirror suggested the use of a second laser, the CWIRL, to photodissociate ions produced by the PIRL. For the double laser experiment, the sample was

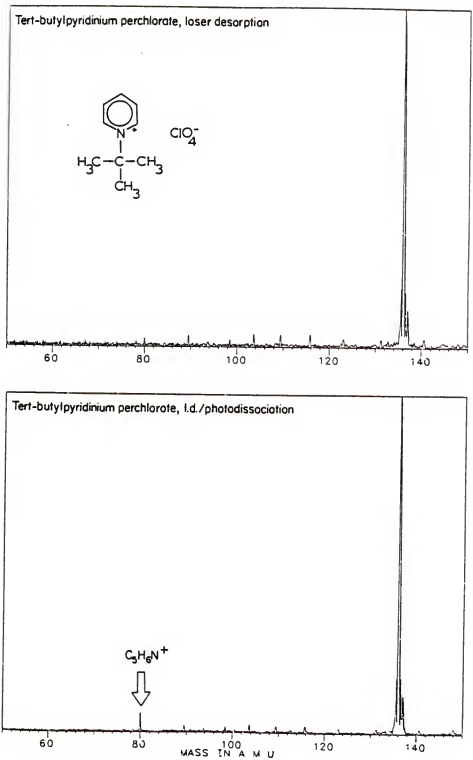

Figure 7.6. Top. Tertbutylpyridinium cation formed by laser desorption from its perchlorate salt. Bottom. Fragmentation achieved with a single laser pulse from a pulsed CO_2 laser, all other conditions identical to the top spectrum.

prepared on the SWT described above and inserted into the vacuum chamber through the solids probe inlet. As shown in Figure 7.2 the PIRL beam was directed into the cell using the normal desorption optics and ions were desorbed in the usual manner. The CWIRL beam entered the vacuum chamber through the salt window mounted on the SWT. Ions were formed from a focused PIRL pulse and after a delay of 1 - 3 s to allow the initial pressure burst due to desorbed neutrals to dissipate the CWIRL irradiated the ions for 0.5 - 3 s until significant photodissociation was observed.

The SWT could be rotated and divided into eight different areas where there was no overlap of the PIRL beam. Sample on each area produced significant ion signal for a range of 3 - 20 laser pulses depending on the sample and preparation characteristics. The standard experimental method employed involved collection of a LD, LD/PD, and second LD mass spectrum, giving a reference spectrum before and after the LD/PD spectrum and eliminating the possibility of the photofragments originating from some unknown source. Results for several samples are discussed below.

N,N'-bis(4,6-dimethylsalicylidene)-4-trifluoromethyl-o-phenylendiiminato cobalt (II) (CoSALOPH). This compound was selected as a test case since its PD pathways were known (see Equation 7.2 and Figure 7.4) and significant amounts of $(M+H)^+$ were observed following laser desorption. Photodissociation behavior observed following laser desorption was identical to that seen when electron impact was used to produce the ions (Equation 7.2).

Sucrose. Observation of the molecular ion produced by LD (Van Der Peyl, 1982)) and LD followed by EI (Hein, 1986) have been reported for sucrose. The negative ion mass spectrum following laser desorption reveals a $(M-1)^-$ ion at m/z 341. When irradiated this ion dissociates with production of ions at m/z 251, 249, 179 and 161 as shown in Figure 7.7. The ion at m/z 161 corresponds to the loss of a water molecule from one monosaccharide unit. The ion at m/z 179 most likely results from loss of one monosaccharide unit. Since glucose and fructose have identical empirical formulae it is not possible at this time to assign one or the other identity to this ion. These two fragment ions discussed above (m/z 179 and m/z 163) were observed in the negative LD/EI mass spectrum (Hein and Cody, 1986) of sucrose. The fragment ions with m/z 251 and m/z 247, however, are unique photodissociation products. The ions formed at m/z 251 and 247 correspond to loss of $C_3H_6O_3$, and $C_3H_4O_3$ respectively, suggesting that one of the monosaccharide chains may have opened as a result of ionization; otherwise photodissociation brings about the cleavage of two bonds. It is not known at this time whether these ions are produced directly from the $(M-1)^-$ ion or from consecutive PD reactions.

Hesperidin. In the negative ion LD mass spectrum of this compound an ion of m/z 612 was produced from the sodium salt of hesperidin phosphoric acid ester. This ion was observed to dissociate by loss of the attached sugar to

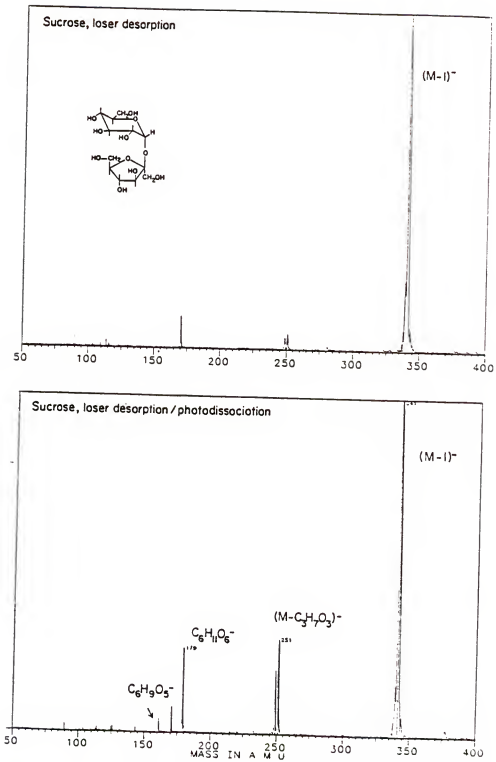

Figure 7.7. Top. Sucrose $(M-H)^-$ ion formed by laser desorption. Bottom. Fragmentation achieved with a continous wave CO_2 laser, all other conditions identical to the top spectrum.

produce an ion at m/z 301 when irradiated by the CWIRL laser as shown in Figure 7.8.

$$m/z\ 617 + nhv \text{ ---> } m/z\ 301 \qquad (7.5)$$

N-2-(5,5-diphenyl-2,4-imidazolidinedionyl-3-ethyl)-7-acetoxy-1-napthyl sulfonamide. This substituted sulfonamide has a molecular weight of 543 amu and in the positive LD mass spectrum two ions at m/z 566 and m/z 582 corresponding to attachment of potassium and sodium ions, respectively were observed. No significant PD was seen for either of these two ions. In the negative ion LD mass spectrum an ion at m/z 500 originating from loss of C_2H_3O was observed. This ion photodissociated when irradiated by the CWIRL to produce an ion at m/z 251 (see Figure 7.9).

$$m/z\ 500 + nhv \text{ ---> } m/z\ 251 \qquad (7.6)$$

High resolution mass analysis of the ion at m/z 251 indicated that it has the empirical formula $C_{15}H_{11}N_2O_2$.

Conclusions

The feasibility of using laser photodissociation to further fragment ions produced by laser desorption has been demonstrated for moderate molecular weight compounds. This technique should work equally well for both positive and negative ions formed by laser desorption. However, for the compounds reported here, negative ion laser desorption usually produced much higher intensities of molecular or pseudo-molecular ions than the corresponding positive ion mode. Applications of visible light (Bowers et al., 1986) and two-photon (Dunbar anf Ferrara, 1985) PD have been

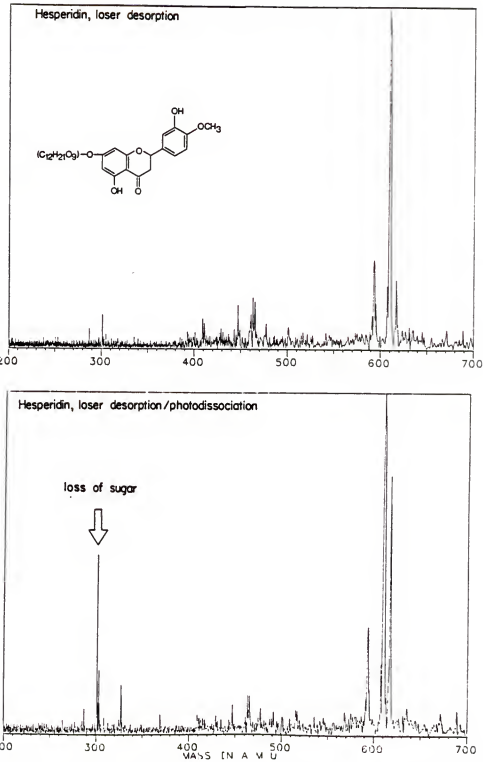

Figure 7.8. Top. Hesperidin negative ions fromed by laser desorption. Bottom. Fragmentation achieved with a continous wave CO_2 laser, all other conditions identical to the top spectrum.

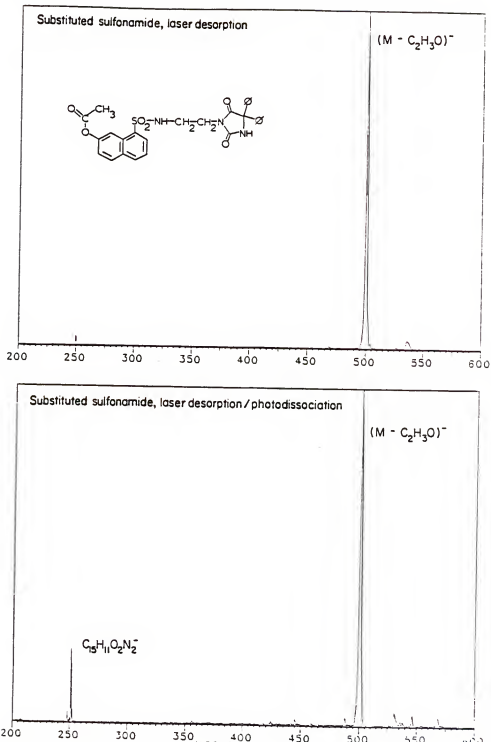

Figure 7.9. Top. N-2-(5,5-diphenyl-2,4-imidazolidine-dionyl-3-ethyl)-7-acetoxy-1-napthyl sulfonamide negative ion formed by laser desorption. Bottom. Fragmentation achieved with a continous wave CO_2 laser, all other conditions identical to the top spectrum.

demonstrated and could be adapted for the photodissociation of laser desorbed ions. Further extensions of this work could include the use of visible and ultraviolet lasers to further fragment large ions such as those produced by the laser desorption technique.

CHAPTER 8
CONCLUSION

General

Infrared multiphoton dissociation of gaseous ions is made possible through the use of Fourier transform ion cyclotron mass spectrometry. The main benefit of this type of mass spectrometry is the ability to store and irradiate ions for up to several seconds, a requirement when continuous wave lasers are employed because the irradiation period must exceed many milliseconds to allow significant dissociation. The technique of infrared multiphoton dissociation is particularly useful for certain applications. Data about both the structure and the energetics of small gaseous ions formed from alcohols, amines, diols, esters and ethers can be obtained.

The technique of infrared multiphoton dissociation can also be applied to differentiate isomeric ions by observing either the photodissociation wavelength dependence or the products of the photodissociation. While this technique does not yield the extensive fragmentation observed with collision-induced dissociation, information about the lowest activation energy, not uniquely determined by other means, can be obtained. In addition, the technique of infrared multiphoton dissociation allows the study of ions of

moderate mass (m/z 300-600) with their many degrees of freedom, since they often possess broad absorption regions in the infrared. Thus, infrared multiphoton dissociation can yield information about a wide variety of ions.

Extensions For Further Work

At present infrared multiphoton dissociation is an excellent source of qualititative information about gaseous ions, since often greater than 50 percent dissociation is observed. However, frequently the quantitative data are not as reliable, and refinement of this information is one important extension of this work. One of the problems in obtaining accurate quantitative data is the interference of ion/molecule back-reactions with the measurement of dissociation. The effects of these ion/molecule reactions can be lessened by lowering the operating pressure inside the mass spectrometer or shortening the irradiation period. However, these steps have as a disadvantage a reduction of the ion signal and a subsequent decrease in the amount of dissociation. One solution to this problem would be the use of high-power pulsed lasers where the pulse width is on a time scale much shorter than that of the ion/molecule reactions.

Another problem in obtaining accurate quantitative data is the difficulty in the optimization of laser conditions. However, by monitoring the laser beam as it exits the cell, this uncertainty about laser conditions can be avoided. The design and use of a cell which allows the laser beam to pass

through it without impinging on any surfaces would permit this sort of monitoring.

Another extremely worthwhile extension of this work would be to allow the irradiation of ions over a much greater wavelength region. Other wavelengths in the infrared region could be obtained through the use of special isotopic gas mixtures in the current lasers. The use of other types of lasers not limited to the infrared region could also be used to irradiate ions.

BIBLIOGRAPHY

Allemann, M.; Kellerhals, H.; Wanczek, K.-P. Chem. Phys. Lett. 1980, 75, 328.

Allemann, M.; Kellerhals, H.; Wanczek, K.-P. Int. J, Mass Spectrom. Ion Proc. 1983, 46, 139.

Ambartzumiam, R.V.; Letokhov, V.S. In "Chemical and Biochemical Applications of Lasers", Vol. 3, Academic Press: New York, 1979, and references therein.

Amster, I.J.; Baldwin, M.A.; Cheng, M.T.; Procter, C.J.; McLafferty, F.W. J. Am. Chem. Soc. 1983, 105, 1654.

Amster, J.I.; McLafferty, F.W.; Castro, M.E.; Russel, D.H.; Cody R.B.; Gahaderi, S. Anal. Chem. 1986, 58, 485.

Aue, D.H.; Bowers, M.T. In "Gas Phase Ion Chemistry"; Vol. 2, Academic Press: New York, 1979, p.1.

Ausloos, P. J. Am. Chem. Soc. 1981, 103, 3931.

Bagratashvili, V.N.; Kuzmin, M.V.; Letokhov, V.S.; Stuchebrukhov, A.A. Chem. Phys. 1985, 97, 13.

Baldeschwieler, J.D. Science 1968, 159, 263.

Baykut, G.; Eyler, J.R. Trends in Anal. Chem. 1986, 5, 44.

Baykut, G.; Watson. C.H.; Eyler, J.R. J. Am. Chem Soc. 1985, 107, 8036.

Beauchamp, J.L.; Dunbar, R.C., J. Am. Chem. Soc. 1970, 92, 1477.

Black, J.G.; Kolonder, P.; Schultz, M.J.; Yablonovitch, E.; Bloembergen, N. Phys. Rev. 1979, A19, 704.

Black, J.G.; Yablonovitch, E.; Bloembergen, N.; Makamel, S. Phys. Rev. Lett. 1977, 38, 1131.

Boer, F.P.; Shannon, T.W.; McLafferty, F.W. J. Am. Chem. Soc. 1968, 90, 7239.

Bohringer, H.; Durup-Ferguson, M.; Fahey, D.H.; Fehsenfeld, F.C.; Ferguson, E.E. J. Chem. Phys. 1983, 79, 4201.

Bohringer, H.; Durup-Ferguson, M.; Freguson, E.E.; Fahey, D.H. Planet. Space Sci. 1983, 31, 483.

Bomse, D.S.; Beauchamp, J.L. J. Am. Chem. Soc. 1981, 103, 3292.

Bomse, D.S.; Berman, D.W.; Beauchamp, J.L. J. Am. Chem. Soc. 1981, 103, 3967.

Bowen, R.D.; Williams, D.H.; Hvistendahl, G. J. Am. Chem. Soc. 1977, 99, 7509.

Bomse, D.S.; Woodin, R.L.; Beauchamp, J.L. In "Advances in Laser Chemistry"; Zewail, A.H., Ed.; Springer: Berlin, 1978, p. 362.

Bomse, D.S., Woodin, R.L., Beauchamp, J. Am. Chem. Soc. 1979, 101, 5503.

Bowen, R.D. J. Chem. Soc., Perkin Trans. II 1982, 409, 1219.

Bowers, W.D.; Delbert, S.-S.; McIver, R.T. Anal. Chem. 1986, 54, 969.

Brill, F.W.; Eyler, J.R. J. Phys. Chem. 1981, 85, 1091.

Burlingame, A.L.; Baillie, T.A.; Derrick, P.J. Anal. Chem. 1986, 58, 165R.

Cantanzarite, J.H.; Haas, Y.; Reisler, H.; Wittig, C. J. Chem. Phys. 1983, 78, 5506.

Chapman, J.R., "Practical Organic Mass Spectrometry"; Wiley: Chichester, 1985

Cody, R.B.; Freiser, B.S. Int. J. Mass Spectrom. Ion Phys. 1982, 41, 199.

Cody, R.B.; Burnier, R.C.; Freiser, B.S. Anal. Chem. 1982, 54, 96.

Cody, R.B.; Burnier, R.C.; Cassady, C.J.; Freiser, B.S. Anal. Chem. 1982, 54, 2225.

Comisarow, M.B. J. Chem. Phys. 1977, 69, 4097.

Comisarow, M.B. Analyt. Chim. Acta 1985, 178, 1.

Comisarow, M.B.; Marshal, A.G. Chem. Phys. Lett., 1974, 25, 282.

Conzemius, R.J.; Capellen, R.J. Int. J. Mass Spectrom. Ion Phys. 1980, 34, 197.

Cooks,G., Ed., "Collision Spectroscopy"; Plenum: New York, 1978.

Cooley, J.W.; Tukey, J.W. Math. Comput. 1965, 19, 297.

Dobler, W.; Howorka, F.; Lindinger, W. Plasma Chem. Plasma Processing 1983, 2, 353.

Dobler, W.; Ramler, H.; Villinger, H.; Howorka, F.; Lindinger, W. Chem. Phys. Lett. 1983, 97, 553.

Dunbar, R.C. Spectrochim. Acta. 1975, 31A, 234.

Dunbar, R.C. In "Gas Phase Ion Chemistry", Vol.2; Bowers, M.T., Ed.; Academic press: New York, 1979, p. 181.

Dunbar, R.C. In "Ionic Processes in the Gas Phase"; Almoster-Ferreira, M.A., Ed.; NATO/ASI Series De Riedel: Dordrecht, Holland, 1984, p. 179.

Dunbar, R.C.; Ferrara, J. J. Chem. Phys. 1985, 83, 6229.

Eyler, J.R. J. Am. Chem. Soc. 1976, 98, 6831.

Eyler, J.R.; Campana, J.E. Int. J. Mass Spectrom. Ion Phys. 1983/1984, 55, 171.

Eyler, J.R.; Richardson, D.E. J. Am. Chem. Soc. 1985, 107, 6130.

Fetterolf, D.D.; Yost, R.A.; Eyler, J.R. Org. Mass Spectrom. 1984, 19, 104.

Ferguson, E.E. In "Swarms of Ions and Electrons", Lindinger, W.; Mark, T.D.; Howorka, F., Ed.s.; Springer: Vienna, 1984.

Ferguson, E.E.; Adams, N.G.; Smith, D.; Alge,E. J. Chem. Phys. 1984, 80, 6095.

Franklin, J.L.; Dillard, J.G.; Rosenstock, H.M.; Herron, J.T.; Draxl, K.; Field, F.H. "Ionization Potentials, Appearance Potentials and Heats of Formation of Gaseous Ions", NSRDS-NBS 26: Washington, D.C., 1969.

Freidman, H. In "Laser-Induced Processes in Molecules", Kompa, K.L.; Smith, S.D., Ed.s.; Springer: Berlin, 1979.

Gaskell, S., Ed. "Mass Spectrometry in Biomedical Research"; Wiley: New York, 1986.

Gear, C.W. In "Applications and Algorithms in Science and Engineering"; Science Research Associates: Chicago 1978.

Glosik, J.; Rakshitt, A.B.; Twiddy, N.D.; Adams, N.G.; Albritton, D.L.; Smith, D. J. Phys. 1978, B11, 3365.

Grant, E.R.; Schultz, P.A.; Sudbo, Aa.S.; Shen, Y.R,; Lee, Y.T. Phys. Rev. Lett. 1978, 40, 115.

Griffiths, I.W.; Harris, F.M.; Beynon, J.H. Int. J. Mass Spectrom. Ion Phys. 1982, 42, 77.

Grimsrud, E.P.; Caldwell, G.; Chowdhury, S.; Kerbale, P. J. Am. Chem. Soc. 1985, 107, 4627.

Gross, M.L.; Russel, D.H.; Aerni, R.J.; Broncyk, S.A. J. Am. Chem. Soc. 1977, 99, 3603.

Haas, Y; Lifshitz, C. Chem. Phys. Lett. 1983, 97, 467.

Haas, Y.; Reisler, H.; Wittig, C. J. Chem. Phys. 1982, 77, 5527.

Hartford, A.Jr. Chem. Phys. Lett. 1978, 3, 503.

Hein, R.E.; Cody, R.B., Nicolet Instrument Corp., unpublished results, 1986.

Hillenkamp, F. In "Ion Formation from Organic Solids", Benninghoven, A., Ed.,; Springer-Verlag: Berlin, 1983.

Huber, K.P.; Hertzberg, G. "Molecular Spectra and Molecular Structure, IV. Constants of Diatomic Molecules "; Van Nostrand-Rhinold: New York, 1979.

Hughes, R.J.; March, R.E.; Young, A.B. Int. J. Mass Spectrom. Ion Phys. 1982, 42, 255.

Ibuki, T.; Sugita, N. J. Chem.Phys. 1983, 79, 5392.

Jackson, J.A.A., Lias, S.C.; Ausloos, P. J. Am. Chem. Soc. 1977, 99, 7515.

Jasinski, J.M.; Brauman, J. J. Chem. Phys. 1980, 73, 619.

Jasinski, J.M.; Rosenfeld, R.N.; Meyer, F.K., Brauman, J.I. J. Am. Chem. Soc. 1982, 104, 652.

Johlman, C.L.; White, R.L.; Wilkins, C.L. Mass Specrtom. Rev., 1983, 2, 389.

Johnson, J.V.; Yost R.A. University of Florida, unpublished results.

Kambara, H. In "Mass Spectrometry in the Health and Life Sciences"; Burlingame, A.L,; Castagnoli, N., Jr., Eds.; Elsevier: Ansterdam, 1985, p. 65.

Karasek, F., Ed. "Mass Spectrometry in Enviromental Sciences"; Plenum Press: New York, 1985.

Kemper, P.R.; Bowers, M.T. J. Chem. Phys. 1984, 81, 2634.

Keyes, B.G.; Harrison, A.G. Org. Mass Spectrom. 1974, 9, 221.

Kim, M.S.; Dunbar, R.C. Chem. Phys. Lett. 1979, 60, 247.

Kuehlewind, H; Neusser, H.J.; Schlag, E.W. J. Chem. Phys. 1984, 88, 6104.

Laude, D.A.Jr.; Johlman, C.L.; Brown, R.S.; Weil, D.A.; Wilkins, C.L. Mass Spectrom. Rev. 1986, 5, 107.

Lee, Y.T.; Shen, Y.R. Phys. Today 1976, 33, 52.

Lehman, T.A.; Bursey, M.M. "Ion Cyclotron Resonance Spectrometry"; John Wiley & Sons: New York, 1976.

Lev, N.B.; Dunbar, R.C. Chem. Phys. 1983, 80, 367.

Levsen, K.; Schwartz,H. Mass Spectrom. Rev. 1983, 3, 1251.

Levy, D.H. In " Advances in Chemical Physics"; Jortner, J.; Levine, R.; Rice, S.A., Eds., Wiley: New York, 1981, Vol 47, Part 1.

Lindholm, E.; Asbrink, L. "Molecular Orbital and their Energies Studied by Semiempirical HAM Methods"; Springer-Verlag: Berlin, 1985.

Long, J.; Munson, B.J. J. Am. Chem. Soc. 1973, 95, 2427.

Lossing, F.P.; Holmes, J.L. J. Am. Chem. Soc. 1984, 106, 6917.

March, J. "Advanced Organic Chemistry: Reactions, Mechanisms, and Structure"; McGraw-Hill: New York, 1977, p.279.

Mark, T.D. In "Electron-Molecule Interactions and Their Applications", Vol. 1; Chistophorou, L.G., Ed.; Academic Press: New York, 1984.

McCrey, D.A.; Ledford, E.B., Jr.; Gross, M.L. Anal. Chem. 1982, 54, 1435.

McFarland, M.; Albritton, D.J.; Fehsenfeld, F.C.; Fergeson, E.E.; Schmeltekopf, A.L. J. Chem. Phys. 1973, 59, 6610.

McLafferty, F.W. Anal. Chem. 1959, 31, 82.

McLafferty, F.W. "Interpretation of Mass Spectra"; University Science Books: Mill Valey, California, 1960.

Moet-Ner, M. J. Am. Chem. Soc. 1983, 105, 4906.

Morgenthaler, L.N. Ph.D. dissertation, University of Florida, 1979.

Morgenthaler, L.N., Eyler, J.R. J. Chem. Phys. 1979, 71, 1486.

Morgenthaler, L.N., Eyler, J.R. J. Chem. Phys. 1981, 74, 4356.

Moylan, C.R.; Brauman, J.I. J. Am. Chem. Soc. 1982, 107, 5527.

Mukhtar, E.S.; Griffiths, I.W.; Harris, F.M.; Beynon, J.H. Org. Mass Spectrom. 1981, 16, 51.

Mukhtar, E.S.; Griffiths, I.W.; Harris, F.M.; Beynon, J.H. Int. J. Mass Spectrom. Ion Proc. 1982, 42, 77.

Nobes, R.H.; Rodwell, W.R.; Bouma, W.J.; Radom, l. J. Am. Chem. Soc. 1981, 103, 1913.

Orth, R.G.; Dunbar, R.C.; J. Am. Chem. Soc. 1982, 104, 5617.

Pandolfi, R.S.; Gobeli, D.A.; Lurie, J.; El-Sayed, M.A. Laser Chem., 1983, 3, 29.

Prisant, M.G.; Rettner, C.T.; Zare, R.N. J. Chem. Phys. 1984, 81, 2699.

Rosenfeld, R.N.; Jasinski, J.M.; Brauman, J.I. J. Am. Chem. Soc. 1983, 105, 658.

Rosenstock, H.M.; Draxl, K.; Steiner, B.W.; Herron, J.T.; J. Phys. Ref. Data 1977, 6, Suppl. 1.

Rowe, B.R.; Fahey, D.H.; Fehsenfeld, F.C.; Albritton, D.L. J. Chem. Phys. 1980, 73, 194.

Sheil, M.M.; Derrick, P.J. Org. Mass Spectrom. 1985, 20, 430

Smith, D.; Adams, N.G. In "Gas Phase Ion Chemistry", Vol. 1; Bowers, M.T., Ed.; Academic Press: New York, 1979, p. 41.

Smith, J.S.; McLafferty, F.W. Org. Mass Spectrom. 1971, 5, 483.

Tabet, J.-C.; Cotter, R.J. Int. J. Mass Spectrom. Ion Phys. 1983, 54, 151.

Tamir, M.; Levine, R.D. Chem. Phys. Lett. 1977, 46, 208.

Thorne, L.R.; Beauchamp, J.L.; in Bowers, M.T.(Ed.) "Gas Phase Ion Chemistry", Vol. 3; Academic Press: New York, 1984, 41.

Van Bremann, R.B.; Snow, M.; Cotter, R.J. Int. J. Mass Spectrom. Ion Phys. 1983, 49, 35.

Van Der Peyl, G.J.Q.; Haverkamp, J.; Kistemaker, Int. J. Mass Spectrom. Ion Phys. 1982, 42, 125.

Watson, C.H.; Baykut, G.; Battiste, M.A.; Eyler, J.R. Analyt. Chim. Acta 1985, 178, 125.

Watson, J.T. "Introduction to Mass Spectrometry", 2nd ed; Raven Press: New York, 1985.

Wight, C.A.; Beauchamp, J.L. J. Am. Chem. Soc. 1979, 103, 6499.

Wilkins, C.L.; Weil, D.A.; Yang, C.L.C.; Ijames, C.F. Anal. Chem. 1985, 47, 520.

Woodin, R.L.; Bomse, D.S.; Beauchamp, J.L. J. Am. Chem. Soc. 1978, 100, 3224.

Woodin, R.L.; Bomse, D.S.; Beauchamp, J.L. Chem. Phys. Lett. 1979, 63, 630.

Yost, R.A.; Enke, C.G. Anal. Chem. 1979, 51, 1251A.

Young, H.D. In "Statistical Treatment of Experimental Data", McGraw-Hill: New York, 1962.

BIOGRAPHICAL SKETCH

Clifford Hunter Watson was born on June 21, 1960, in Brunswick, Georgia, and spent his childhood years exploring Georgia's coastal marshes. He attended the Glynn County public schools and graduated from high school in 1978. He then went on to Georgia College in Milledgeville and received a Bachelor of Science degree in chemistry in 1982.

In the fall of 1982, he began graduate studies at the University of Florida in Gainesville. A year later, he began working in Dr. John Eyler's lab in the area of laser photochemistry. He met his wife, Sonja Rasmussen, and they were married on December 29, 1984. He will complete his graduate studies during the summer of 1986.

Upon graduation, he plans to begin a post-doctoral position with Dr. Eyler, while his wife studies medicine at the University of Florida.

I certify that I have read this study and that in my opinion it conforms to acceptable standards of scholarly presentation and is fully adequate, in scope and quality, as a dissertation for the degree of Doctor of Philosophy.

John R. Eyler, Chairman
Professor of Chemistry

I certify that I have read this study and that in my opinion it conforms to acceptable standards of scholarly presentation and is fully adequate, in scope and quality, as a dissertation for the degree of Doctor of Philosophy.

Richard A. Yost
Associate Professor of Chemistry

I certify that I have read this study and that in my opinion it conforms to acceptable standards of scholarly presentation and is fully adequate, in scope and quality, as a dissertation for the degree of Doctor of Philosophy.

Willis B. Person
Professor of Chemistry

I certify that I have read this study and that in my opinion it conforms to acceptable standards of scholarly presentation and is fully adequate, in scope and quality, as a dissertation for the degree of Doctor of Philosophy.

Charles L. Beatty
Professor of Materials Science and Engineering

This dissertation was submitted to the Graduate Faculty of the Department of Chemistry in the College of Liberal Arts and Sciences and to the Graduate School and was accepted as partial fulfillment of the requirements for the degree of Doctor of Philosophy.

December 1986

_____

Dean, Graduate School